Measuring the heterogeneity of the coseismic stress change following the 1999 Mw7.6 Chi-Chi earthquake

David Marsan, Guillaume Daniel

Measuring the heterogeneity of the coseismic stress change following the 1999 M_w7.6 Chi-Chi earthquake

D. Marsan[1] and G. Daniel[2]

Received 24 July 2006; revised 6 December 2006; accepted 5 April 2007; published 7 July 2007.

[1] Seismicity quiescences are expected to occur in places where the stress has been decreased, in particular following large main shocks. However, such quiescences can be delayed by hours to years and be preceded by an initial phase of earthquake triggering. This can explain previous analyses arguing that seismicity shadows are rarely observed, since they can only be seen after this triggering phase is over. Such is the case of the main rupture zone, which experiences the strongest aftershock activity despite having been coseismically unloaded by up to tens of bars. The 1999 M_w7.6 Chi-Chi, Taiwan earthquake is characterized by the existence of several such delayed quiescences, especially off the Chelungpu fault on which the earthquake took place. We here investigate whether these delays can be explained by a model of heterogeneous static-stress transfer coupled with a rate-and-state friction law. We model the distribution of coseismic small-scale stress change τ by a Gaussian law with mean $\bar{\tau}$ and standard deviation σ_τ. The latter measures the level of local heterogeneity of the coseismic change in stress. The model is shown to mimic the earthquake time series very well. Robust inversion of the $\bar{\tau}$ and σ_τ parameters can be achieved at various locations, although on-fault seismicity has not been observed for a sufficiently long time to provide more than lower bounds on those estimates for the Chelungpu fault. Several quiescences have delays that can be well explained by local stress heterogeneity, even at relatively large distances from the Chi-Chi earthquake.

Citation: Marsan, D., and G. Daniel (2007), Measuring the heterogeneity of the coseismic stress change following the 1999 M_w7.6 Chi-Chi earthquake, *J. Geophys. Res.*, *112*, B07305, doi:10.1029/2006JB004651.

1. Introduction

[2] Static-stress triggering predicts that off-fault seismicity can either be turned on or off with roughly equal probability, depending on the location and orientation of the target fault relative to the main fault. However, several studies have pointed out the absence or paucity of seismicity shadows after large main shocks [*Parsons*, 2002; *Marsan*, 2003; *Felzer and Brodsky*, 2005; *Marsan and Nalbant*, 2005; *Daniel et al.*, 2006; *Mallman and Zoback*, 2007]. While immediate, significant seismicity decreases are indeed very rare (see *Dieterich et al.* [2000], *Toda and Stein* [2003], and *Woessner et al.* [2004] for exceptions), late quiescences typically delayed by months have been reported in several studies: about 4 months on the locked segment in Parkfield following the 1983 Coalinga earthquake [*Toda and Stein*, 2002], 6 months in extended areas of the Landers rupture zone, at shallow depths [*Ogata et al.*, 2003], a few months at several locations following the Chi-Chi earthquake [*Ma et al.*, 2005], and 4 months after the Izmit earthquake at Yalova [*Daniel et al.*, 2006]. Relative late quiescences during aftershock sequences have also been observed following $M6^+$ earthquakes in Japan by *Ogata* [2001].

[3] It is not clear whether such delayed quiescences are triggered or at least causally connected to the main shock. For example, *Ogata et al.* [2003] proposed that the quiescence they observed after Landers could be due to aseismic slip occurring on the fault that was to rupture 6 years later during the Hector Mine earthquake. More generally, *Felzer and Brodsky* [2005] argued that quiescences happen at random, with spatial structures that are not coherent with static-stress triggering modeling, so that they could not be attributed to the main shock. In the case of delayed quiescences, causality is indeed an issue, as with increasing delay it becomes more and more difficult to reject the possibility that some postseismic process, hence something else than the coseismic stress change itself, could have caused them.

[4] The fact that quiescences can be delayed is however not too surprising; such a phenomenon is expected to occur on the main fault, which can become silent after years of strong aftershock activity. The initial phase of seismicity increase (aftershocks) is then attributed to heterogeneity of slip, hence of stress, while the latter phase of quiescence is a signature of the overall stress drop caused by the main

[1]Laboratoire de Géophysique Interne et Tectonophysique, Université de Savoie, Le Bourget du Lac, France.
[2]Laboratoire de Géophysique Interne et Tectonophysique, Observatoire de Grenoble, Grenoble, France.

0148-0227/07/2006JB004651$09.00

shock. Following this line of thought, *Helmstetter and Shaw* [2006] and *Marsan* [2006] used the rate-and-state friction model [*Dieterich*, 1979, 1994; *Ruina*, 1983] to show that realistic levels of coseismic slip can indeed well explain the occurrence of delayed quiescences. Also, Helmstetter and Shaw demonstrated that the initial aftershock phase is then characterized by (low) p values correlated with the degree of stress heterogeneity.

[5] A question is then, can off-fault quiescences also be delayed due to heterogeneous stress changes? As shown by *Helmstetter and Shaw* [2006] and *Marsan* [2006], stress heterogeneity created by variability in slip is likely to be too low past about one fifth to one half of the rupture length away from the main fault to create any delayed seismicity shadows. Another source for roughening the coseismic stress field at greater distances must then be invoked, as for example structural heterogeneity in heavily damaged and fractured zones, for which local stress concentrations are expected. As already discussed by *Marsan* [2006], static-stress modeling is based on computing smooth stress fields; it is therefore unlikely to explain those seismicity changes caused by small-scale heterogeneous stress changes, as in the case of delayed quiescences.

[6] This paper is an attempt at testing whether off-fault coseismic stress heterogeneity can be measured from the time evolution of seismicity, more particularly in case delayed quiescences are observed. To do so, we use the rate-and-state friction model to relate stress and earthquake rates. We examine the Chi-Chi earthquake aftershock sequence, mainly because (1) the seismicity is abundant and monitored by a dense network of stations, and (2) this sequence exhibits several delayed quiescences at various well-identified locations [*Ma et al.*, 2005]. We therefore test whether quiescences which start was typically delayed by months can indeed be modeled as due to stress changes with negative mean but strong spatial variability, hence including small zones of positive stress changes. This study is therefore not a systematic search for seismicity shadows; we rather aim at understanding if immediate shadows could be rare because of the delaying effect caused by stress heterogeneity.

[7] We first present in section 2 the method for measuring the significance of seismicity shadows and for estimating stress heterogeneity and then detail the analysis of the Chi-Chi sequence in section 3. The main conclusion of this work, as further discussed in section 4, is that only a few delayed quiescences are really significant, with some of them that can indeed be well explained by coseismic stress heterogeneity, albeit at distances from the main fault that are large enough to prevent slip spatial variability to play a role in creating such an heterogeneity.

2. Method

2.1. Outline

[8] The objective is to estimate, from an earthquake catalogue, hence from seismicity rates, the distribution of coseismic stress changes. For any given location, we assume a Gaussian distribution of stress; hence only two parameters are sought, the mean stress change $\bar{\tau}$ and the standard deviation σ_τ. It is the latter parameter that measures the local stress variability.

[9] Close to the main shock, i.e., within the rupture zone, the change in seismicity rate caused by the earthquake is generally very clearly seen. In the case of the Chi-Chi earthquake, the seismicity rates were particularly stable in the years prior, so that the vigorous activity following Chi-Chi can be directly related to the main shock. We then simply examine the Omori-Utsu rate decay after Chi-Chi and try to fit this decay by a parameterized model of seismicity depending on parameters $\bar{\tau}$ and σ_τ. We use the rate-and-state friction model of *Dieterich* [1979, 1994] and *Ruina* [1983].

[10] Further away from the mainfault, at distances greater or of the order of about half the rupture length, the seismicity time series is not as strongly influenced by the main shock anymore. Other smaller, local earthquakes can then significantly perturb the seismicity. In order to measure the coseismic stress change caused by Chi-Chi, it is then necessary to account for those perturbations. We then model the 9+ yearlong time series (starting 5 years before and ending 4.4 years after the main shock) by assuming that several earthquakes, rather than just Chi-Chi, can trigger seismicity. Such earthquakes are called "triggers." The main difficulty becomes then to define the number of triggers that are needed to correctly fit the series and to constrain their occurrence times.

[11] In this section, we detail all these issues in a general context. The case of the Chi-Chi earthquake is examined in section 3.

2.2. Rate-and-State Friction Modeling

[12] In order to fit the observed seismicity, we use a model based on rate-and-state friction [*Dieterich*, 1979, 1994; *Ruina*, 1983] with the slowness law [*Dieterich*, 1986]. This model assumes that an infinite population of independent earthquake nucleation sites reacts to changes in stress conditions according to the rate-and-state friction law. The seismicity rate (number of earthquakes per unit time) is defined as

$$\lambda(t) = \frac{\mu}{\gamma(t)\dot{\tau}} \tag{1}$$

with μ the stationary background rate, i.e., the constant rate of earthquake occurrences if the driving stress acting on the faults increases linearly with time, i.e., as in the case of faults only sensitive to the constant tectonic stress loading rate $\dot{\tau}$. Parameter γ is a function such that $d\gamma = dt - \gamma d\tau$ and contains the coupling of the population of nucleation sites to the changes in stress. Time dependence of the seismicity rate $\lambda(t)$ is controlled by the time evolution of this function $\gamma(t)$. We model τ as a quantity uniformly increasing with time $d\tau/dt = \dot{\tau}$ (tectonic loading), to which stress steps $\{\tau_i\}$ occurring at times $\{t_i\}$ are added (sudden stress changes, called triggers). All stresses are normalized and are expressed in units of $A\sigma$, where A is a constitutive parameter of rate-and-state friction with typical value around 0.001 [*Dieterich*, 1994], and σ is the normal stress acting on the fault. All times are in units of $t_a = \frac{A\sigma}{\dot{\tau}}$.

[13] As already detailed in *Marsan* [2006], for a fault initially at steady state and undergoing N stress changes $\{\tau_i\}=\tau_1,\ldots,\tau_N$ at times t_i, the function γ defined in equation (1) is:

$$\gamma(t < t_1) = \frac{1}{\dot{\tau}}$$

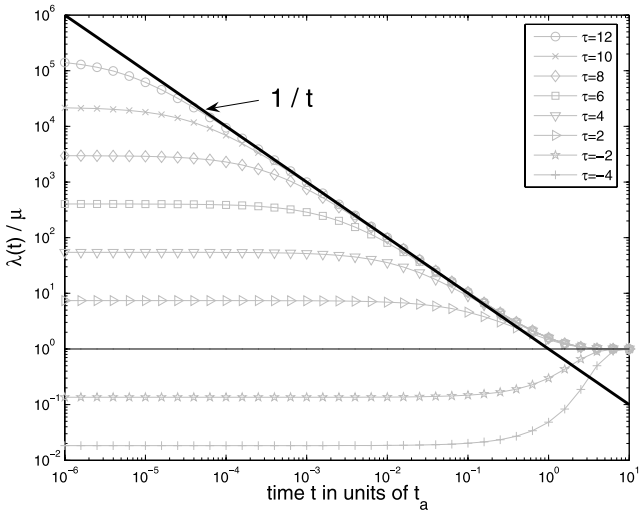

Figure 1. Seismicity rate λ following a main shock causing a stress step τ, for varying values of τ. The rate change λ/μ eventually collapses onto a single $1/t$ curve, until $t \simeq 1$.

$$\gamma(t_1 < t < t_2) = \frac{1}{\dot{\tau}} \times \left\{1 + e^{-(t-t_1)}(e^{-\tau_1} - 1)\right\}$$

$$\gamma(t_2 < t < t_3) = \frac{1}{\dot{\tau}} \times \{1 + e^{-(t-t_1)} \times (e^{-\tau_1-\tau_2} - e^{-\tau_2} + e^{t_2-t_1}(e^{-\tau_2} - 1))\}$$

...

or equivalently

$$\gamma(t_i < t < t_{i+1}) = \frac{1}{\dot{\tau}} \times \left\{1 + e^{-(t-t_1)}\epsilon_i\right\} \tag{2}$$

with ϵ_i recursively computed as:

$$\epsilon_i = \epsilon_{i-1}e^{-\tau_i} + e^{t_i-t_1}(e^{-\tau_i} - 1) \tag{3}$$

starting at $t < t_1$ with $\epsilon_0 = 0$.

[14] In the case of just one trigger acting at time $t = 0$, the seismicity rate jumps from the background rate μ to $\lambda(t = 0^+) = \mu e^{\tau}$ immediately after the earthquake, stays constant until $t \simeq e^{\tau}$, and then branches onto the μ/t curve, hence an Omori-like decay of the rate; see Figure 1. In the following, triggers are used to denote rapid changes in stress that can modify the seismicity; those changes are most generally caused by earthquakes but not always, as will be shown in the case of the Nansan region (section 4.1). Triggers that are not catalogued as earthquakes could independently be identified in geodetic signals if they cause enough surface displacement.

2.3. Variable Stress Steps

[15] We now consider the case of seismicity generated by a set of N triggers at times $\{t_i\}$, with each stress step distributed following a Gaussian distribution with mean $\{\bar{\tau}_i\}$ and standard deviation $\{\sigma_{\tau_i}\}$. More precisely, the seismicity rate $\lambda(t)$ is the sum of an infinite number of (infinitely low) rates on (infinitely small) patches, each behaving independently from the others and undergoing a series of stress steps in which values are randomly and independently drawn among N Gaussian populations $\mathcal{N}(\bar{\tau}_i, \sigma_{\tau_i})$. This amounts to say that λ is the ensemble average of $\lambda(t|\tau_1,\ldots,\tau_N)$ with $\tau_i = \mathcal{N}(\bar{\tau}_i, \sigma_{\tau_i})$ independent of all others τ_j, $j \neq i$. The ensemble average is therefore taken over all the possible stress trajectories. The model is therefore equivalent to computing a path integral for stress random walks with prescribed times of displacements.

[16] Numerically, the computation of $\lambda(t_i < t < t_{i+1})$ is performed by keeping track of the set of values $\epsilon_i^{(k)}$, $1 \leq k \leq N_k$, such that $P(\epsilon_i < \epsilon_i^{(k)}) = k/N_k$. This is done with the following algorithm:

$$t < t_1 : \epsilon_0^{(k)} = 0, \forall k.$$

$$t_1 < t < t_2:$$

$$\epsilon_1^{(k)} = e^{-\tau_1^{(k)}} - 1 \tag{4}$$

with $\tau_1^{(k)}$ such that

$$k/N_k = 1/2 + 1/2 \times \mathrm{erf}\left(\frac{\tau_1^{(k)} - \bar{\tau}_1}{\sqrt{2}\,\sigma_{\tau_1}}\right) \tag{5}$$

Then, starting with $i = 2$:

[17] $t_i < t < t_{i+1}$: N_k^2 values of $\epsilon_i^{(k)}$ are computed as all the combinations involving the N_k values of $\tau_i^{(k)}$ such that

$$k/N_k = 1/2 + 1/2 \times \mathrm{erf}\left(\frac{\tau_i^{(k)} - \bar{\tau}_i}{\sqrt{2}\sigma_{\tau_i}}\right) \tag{6}$$

and the N_k values of ϵ_{i-1}. We thus have

$$\epsilon_i^{(l,m)} = \epsilon_{i-1}^{(l)} e^{-\tau_i^{(m)}} + e^{t_i-t_1}\left(e^{-\tau_i^{(m)}} - 1\right) \tag{7}$$

with both l and m ranging between 1 and N_k. Those N_k^2 values are then sorted by ascending order. This gives a set of N_k^2 increasing values with the property that $P(\epsilon_i < \epsilon_i^{(k)}) = k/N_k^2$, the unique index k now ranging from 1 to N_k^2. A decimation is finally performed, so to only keep one $\epsilon_i^{(k)}$ value every N_k.

[18] Finally, the seismicity rate at time $t_i < t < t_{i+1}$ is computed from the $\epsilon_i^{(k)}$ values as:

$$\lambda(t_i < t < t_{i+1}) = E\left\{\frac{\mu}{1 + e^{-(t-t_1)}\epsilon_i^{(k)}}\right\} \tag{8}$$

$$\Rightarrow \lambda(t_i < t < t_{i+1}) = \frac{1}{N_k}\sum_{k=1}^{N_k} \frac{\mu}{1 + e^{-(t-t_1)}\epsilon_i^{(k)}} \tag{9}$$

[19] For a single trigger, there are three limit cases; see Figure 2, (a) $\bar{\tau} \gg 1$ and $\bar{\tau} \gg \sigma_\tau$, in which case $\lambda \to \mu/t$ which is the maximum rate for a single trigger, as already described in section 2.2; (b) $\bar{\tau} \ll -1$ and $|\bar{\tau}| \gg \sigma_\tau$, for which the rate $\lambda \to \mu e^{\bar{\tau}}$ stays constant until about $t = 1$; (c) $|\bar{\tau}| \ll \sigma_\tau$, for which $\lambda \to \frac{1}{2}\mu/t$; that is, the rate is half the maximum rate.

[20] Robut estimation of parameter σ_τ can only be done when $\bar{\tau} < 0$ and the quiescence is effectively observed. This can imply long observation times if both $|\bar{\tau}|$ and σ_τ are large. When $\bar{\tau} > 0$, this estimation becomes difficult because t_a is then not well constrained, and its error directly impacts on σ_τ. A strong constraint on σ_τ can, however, be obtained in all cases if the seismicity is reliably documented in the very early times (for example, hours) after the main shock. Then, the existence or not of an early stationary regime,

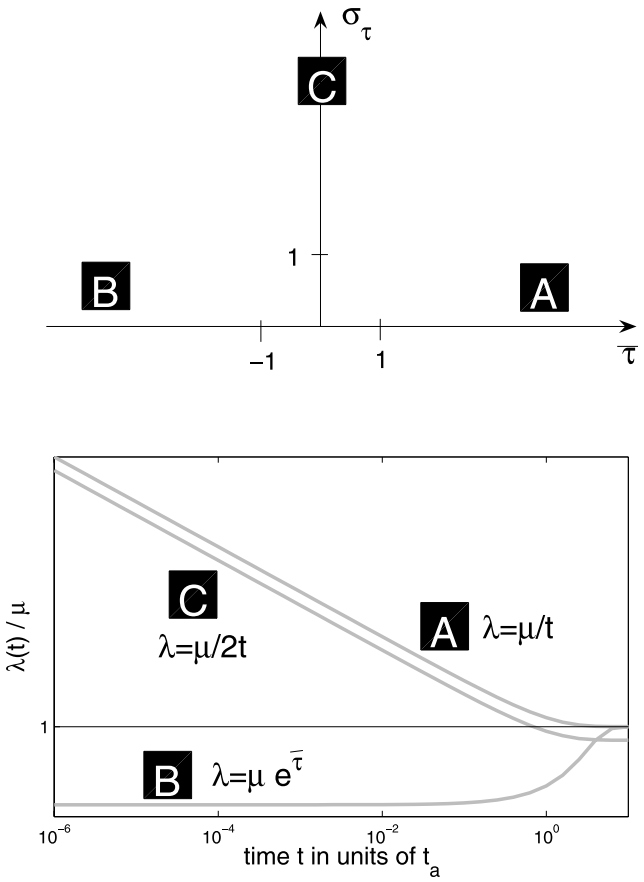

Figure 2. Three limit cases for a single trigger with variable stress step, see text. (a) $\bar{\tau} > 0$, $\sigma_\tau \ll \bar{\tau}$, leading to $\lambda = \frac{\mu}{t}$. (b) $\bar{\tau} < 0$, $\sigma_\tau \ll \bar{\tau}$, leading to $\lambda = \mu e^{\bar{\tau}}$. (c) $\sigma_\tau \gg \bar{\tau}$, leading to $\lambda = \frac{\mu}{2\times t}$ for $t < \frac{t_a}{2}$.

hence of a cut-off timescale (the c parameter in Omori's law), gives strong clues about σ_τ: large values of σ_τ imply no clear cut-off, while $\sigma_\tau = 0$ is characterized by an early stationary regime. Recent observations point toward a vanishingly small c [*Kagan and Houston*, 2005], at least for on-fault seismicity, hence large levels of on-fault stress heterogeneity [*Helmstetter and Shaw*, 2006]. It thus becomes important to examine the seismicity at times as early as possible, despite a quickly varying magnitude of completeness in this time interval. This is discussed in greater length in section 3.2 when studying the stress heterogeneity on the Chi-Chi (Chelungpu) fault.

2.4. A Test of the Method

[21] In order to illustrate and check the validity of the method, a synthetic time series $\{t_i\}$ is simulated as a realization of the rate-and-state model of section 2.3 with five triggers. The model parameters are detailed in Table 1 and were chosen to resemble those obtained for the Nansan region, studied in section 4.1. Figure 3a shows the time series, along with the best fit. The (negative) log likelihood is used as the cost function $J(\theta) = \int dt\lambda(t) - \sum_i \ln\lambda(t_i)$ with

Table 1. Model Parameters for the Synthetic Time Series[a]

Trigger	$\bar{\tau}$	σ_τ
1	1	1
2	2.55	3
3	3	0
4	−0.88	1.89
5	−4.25	5.15

[a]Parameter t_a is equal to 2 (in arbitrary units).

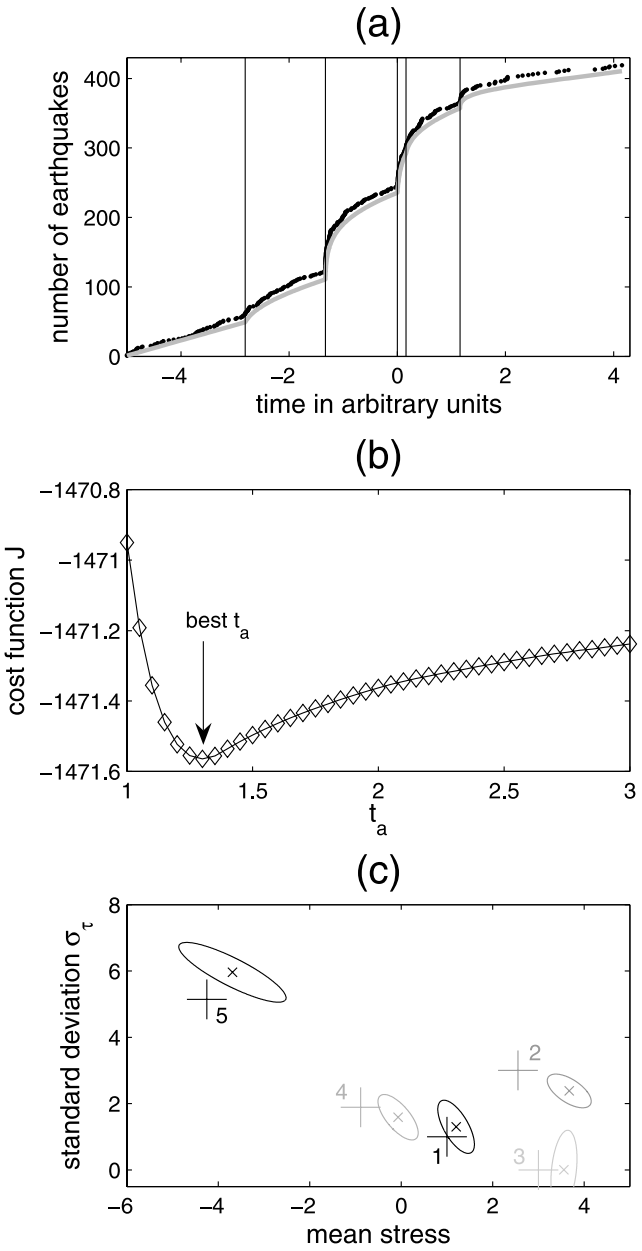

Figure 3. (a) Synthetic time series (black dots) using the parameters of Table 1 and best fit model (gray line). The occurrence times of the five triggers are indicated with vertical lines. (b) Minimum cost function J obtained when inverting the 10 stress parameters ($\bar{\tau}$ and σ_τ for each of the five triggers) at fixed t_a versus t_a. The best t_a is found equal to $\widehat{t_a} = 1.3$. (c) The 10 stress parameters (×), obtained by inversion of the data, and their error ellipses, using the best fit at $\widehat{t_a} = 1.3$, compared to the input parameters (+) of Table 1. The triggers are numbered from 1 to 5. The significant underestimation of t_a ($\widehat{t_a} = 1.3 \pm 0.6$ compared to the input value of $t_a = 2$) causes the stress estimates to depart from the input values.

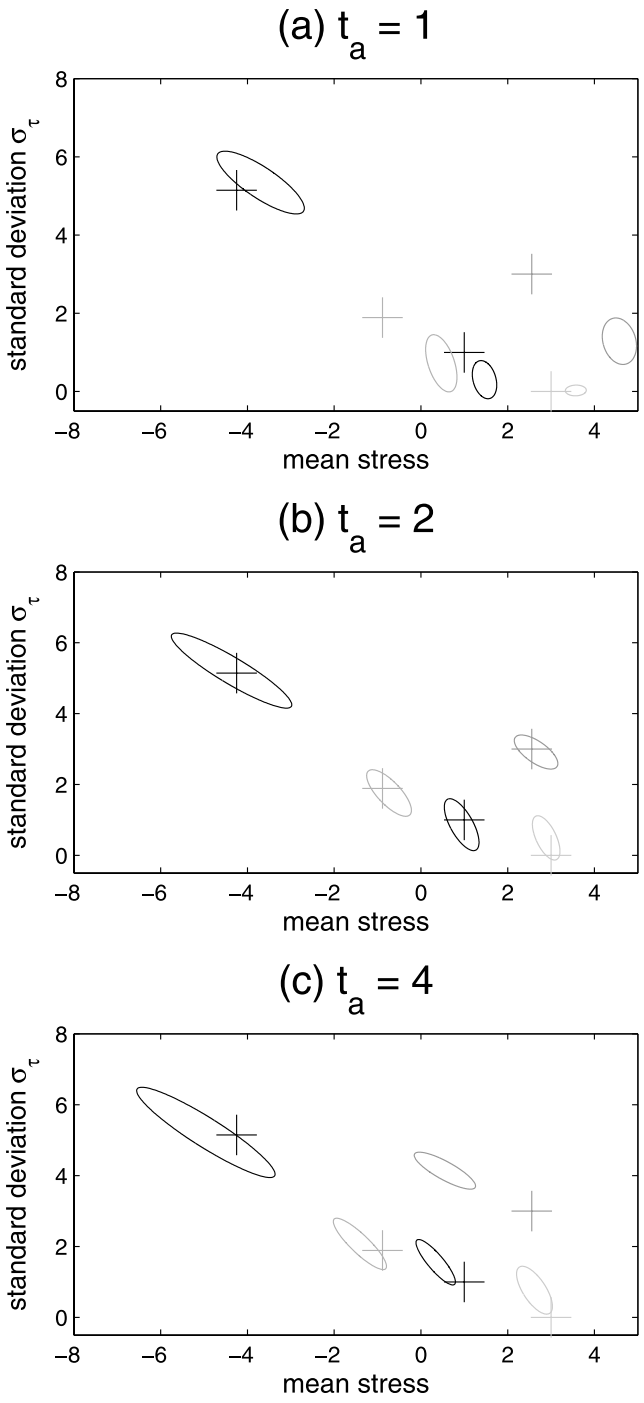

Figure 4. Effect of how under/overestimating t_a affects the values of the inverted stress parameters, results of 100 independent synthetic earthquake time series with parameters of Table 1 and stress parameter inversions for which we fixed parameter $\widehat{t_a}$ to (a) $\widehat{t_a} = 1$, (b) 2, and (c) 4. The actual model t_a parameter is equal to 2. The ellipses are drawn at the $1 - \sigma$ contour, hence in two-dimensional contain $\simeq$46.6% of the 100 sample points.

$\lambda(t)$ defined in equation (9). For each trigger, two parameters are sought ($\bar{\tau}$ and σ_τ). The duration t_a is also inverted. Here since five triggers are considered, a total of 11 parameters are inverted. The best model is obtained by running the inversion on the 10 stress parameters $\{\bar{\tau},\sigma_\tau\}$ at fixed t_a. Regularly spaced values of t_a were tested, and the value $\widehat{t_a}$ yielding the minimum cost function J was kept as the best estimate of t_a, cf. Figure 3b. From this $\widehat{t_a}$, we obtain the best parameter set $\underline{\widehat{\theta}} = \{\widehat{\bar{\tau}}, \widehat{\sigma_\tau}\}$.

[22] Error on the 11 parameters are estimated by perturbing this best parameter set $\underline{\widehat{\theta}} \rightarrow \underline{\theta'} = \underline{\widehat{\theta}} + \underline{\epsilon}$ and performing a quadratic fit of the cost function

$$J = J_0 + \underline{\epsilon} \cdot \partial_{\underline{\theta}} J(\underline{\widehat{\theta}}) + \frac{1}{2}\underline{\epsilon}^T \partial^2_{\underline{\theta}} J(\underline{\widehat{\theta}})\underline{\epsilon} + o(\epsilon^3) \qquad (10)$$

yielding the covariance matrix of the errors $\left[\partial^2_{\underline{\theta}} J(\underline{\widehat{\theta}})\right]^{-1}$. Figure 3c displays the error ellipses in the $(\bar{\tau},\sigma_\tau)$ plane, where each of the five triggers is examined independently; that is, 2×2 covariance matrices are extracted from the full covariance matrix. Typical errors are of the order of ± 1 on stress parameters, while the error on t_a is ± 0.6, hence $\widehat{t_a} = 1.3 \pm 0.6$ compared to the actual value of $t_a = 2$ used for generating the time series.

[23] This test can be extended further in order to check the sensitivity of the inversion to the estimation of t_a. One hundred independent realizations of the model were run, keeping with the same model parameters as of Table 1, and, for each realization, the best parameter set was estimated. This was done by setting $\widehat{t_a}$ to be equal to 1, 2, and 4, and inverting only the remaining 10 (stress) parameters. Figure 4 clearly shows the strong influence of $\widehat{t_a}$. Very generally, for any given trigger, the two parameters $\widehat{\bar{\tau}}$ and $\widehat{\sigma_\tau}$ are anticorrelated, as shown by the shapes of the error ellipses in Figures 3c and 4. Taking a lower value of $\widehat{\bar{\tau}}$ implies that the early triggering rate is underestimated, which can be counter-balanced by an increase in $\widehat{\sigma_\tau}$ since the latter promotes early aftershocks [*Marsan*, 2006; *Helmstetter and Shaw*, 2006]. Underestimating t_a promotes early rates, too, but also causes the quiescence to occur earlier, when $\bar{\tau} < 0$. The estimation mostly sees the first effect, which is compensated by decreasing $\widehat{\sigma_\tau}$, hence $\widehat{t_a}$ and $\widehat{\sigma_\tau}$ are positively correlated, while $\widehat{t_a}$ and $\widehat{\bar{\tau}}$ are anticorrelated. These correlations between the parameters can be directly seen in the error covariance matrix. Figure 4 also shows that too low a value of $\widehat{t_a}$ (for example, Figure 4a) implies larger mean stresses and smaller stress standard deviations.

[24] Such correlations between the parameters are likely to cause problems in estimating the distribution of the stress change. In particular, a significant error in the estimate of t_a can change the sign of the mean stress $\hat{\bar{\tau}}$: a $\widehat{t_a}$ larger than the "true" t_a could lead to an estimated negative mean stress change. It is therefore of great importance in such an analysis to accurately measure how sensitive the results are to perturbations of the estimate $\widehat{t_a}$.

2.5. Measuring Seismicity Rate Changes

[25] As well as measuring the variability in coseismic stress, we also quantify the significance of seismicity shadows when observed. We here follow the approach already documented by *Marsan* [2003], *Marsan and Nalbant* [2005] and *Daniel et al.* [2006]. This method compares a predicted number of earthquakes Λ_0 had the main shock not occurred to the actually observed number Λ_1. The prediction relies on the seismicity model used to mimic the earthquake time series.

[26] More specifically, the model parameter set θ is first optimized $\theta \rightarrow \hat{\theta}$ by fitting the model to the earthquake time

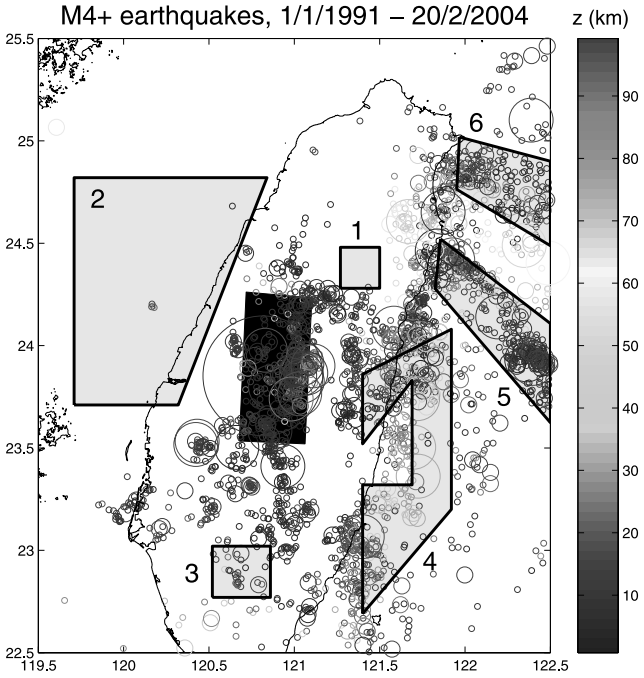

Figure 5. *M*4+ earthquakes in Taiwan, 1991–2004. The Chelungpu fault that ruptured during the Chi-Chi earthquake is sketched by its projection onto the surface, in black. The four areas reported by *Ma et al.* [2005] to have experienced delayed quiescences plus the two additional zones discussed in section 4.5 are shown in gray: (1) Nansan, (2) Taichung, (3) Kaoping, (4) Huathung, (5) Nanao forearc, (6) Okinawa Trough.

series $\{t_1, t_2, \ldots\}$ up to the time of the main shock T_0, according to the cost function $J(\theta) = \int_0 dt\lambda(t) - \sum_{t_i<T_0} \ln\lambda(t_i)$; see section 2.4. The covariance matrix of the error $\Delta\theta$ is estimated by least squares fitting J in the vicinity of the solution $\hat{\theta}$. We then extrapolate the model rate $\lambda(t)$ after the main shock to estimate the predicted rate. The distribution of this predicted rate is found by perturbing $\hat{\theta}$ according to the error $\Delta\theta$. This distribution is finally compared to the real, observed rate. More precisely, for a time interval $[T_1, T_2]$ after the main shock, the number of observed earthquakes N gives the probability density function $f_1(\Lambda_1) = e^{-\Lambda_1}\Lambda_1^N/N!$ of the Poisson mean Λ_1. This density is compared to the null hypothesis, corresponding to the predicted mean Λ_0 computed as $\Lambda_0 = \int_{T_1}^{T_2} dt\lambda(t)$ for the model with parameters $\hat{\theta}$ and error $\Delta\theta$. Finally, the significance of the change is measured by the probability $\mathcal{P} = P(\Lambda_1 > \Lambda_0) = \int_0^\infty d\Lambda_0 f_0(\Lambda_0) \int_{\Lambda_0}^\infty d\Lambda_1 f_1(\Lambda_1)$ that the real rate can be greater than the predicted rate "by chance."

3. Analysis of the Chi-Chi Sequence: On-Fault Heterogeneity of the Stress Change

3.1. General Presentation

[27] On 21 September 1999, the M_w7.6 Chi-Chi earthquake ruptured 80 to 100 km of the Chelungpu thrust fault in Taiwan, with a downdip extension of 35 to 40 km, and caused a ≃10-m maximum offset at the surface [*Shin and Teng*, 2001]. Individual or joint inversions of the coseismic slip distribution, based on strong motion and teleseismic, Global Positioning System (GPS), and Satellite Pour l'Observation de la Terre (SPOT) images, have robustly shown that slip generally increased updip and toward North or similarly that a strong asperity with 15m–20m slip was located about halfway between the hypocenter and the northern end of the rupture [*Iwata et al.*, 2000; *Kikuchi et al.*, 2000; *Ma et al.*, 2000, 2001; *Yoshioka*, 2001; *Dominguez et al.*, 2003; *Zhang et al.*, 2003; *Loevenbruck et al.*, 2004].

[28] We analyze the seismicity as given by the Central Weather Bureau, starting 5 years before and ending 4.4 years after the main shock. Thirteen years of seismicity, including the 1999 Chi-Chi earthquake, are shown in Figure 5. We only consider in this analysis the seismicity starting from September 1994, as changes in detection make the catalogue inhomogeneous before this date. We first focus on the main fault and then in those areas found by *Ma et al.* [2005] to undergo quiescences in the months following Chi-Chi. We both search for seismicity shadows and quantify their statistical significance and measure the level of coseismic stress heterogeneity when possible. The latter is given in units of parameter $A\sigma$ intervening in the rate-and-state friction model rather than in absolute stress values. Typical values of $A\sigma$ have been found elsewhere to be of the order of 0.01 to 0.1 MPa, e.g., in the works of *Toda et al.* [1998] and *Cochran et al.* [2004].

3.2. Stress Heterogeneity on the Ruptured Chelungpu Fault

[29] Following the Chi-Chi earthquake, a strong aftershock activity took place, most particularly at 10 km depth on the main fault where the aftershock rate reaches a maximum; see Figures 6 and 7b. As already noticed by *Ma et al.* [2001], the change in seismicity rate is globally anticorrelated with the coseismic slip distribution; lower rate changes are found around the hypocenter and the patch of large slip located in the northernmost half of the rupture. In the case of Chi-Chi, aftershocks tend to favorably occur in areas of low slip.

[30] Aftershocks cluster at the downdip termination of the rupture (≃30 to 40 km on the y axis of Figure 7b). This, along with the existence of an aseismic decollement at ≃10 km depth [*Loevenbruck et al.*, 2001; *Dominguez et al.*, 2003] and the close similarity in shape of the aftershock time series and the postseismic GPS displacements near the fault, have led *Perfettini and Avouac* [2004] to propose that aftershocks were primarily driven by afterslip on the decollement plane. The transition zone between the aseismic decollement and the locked fault at shallow depth is expected to be short, i.e., kilometric. A different conclusion is reached by *Cattin et al.* [2004], who proposed that the coseismic slip deficit linearly increasing with depth must imply a seismic coupling decreasing from 100 to 0% over the whole 30-km width of the rupture. While aftershocks indeed cluster at 10-km depth, the seismicity rate change is maximum at shallower depth, cf. Figure 7c. The distribution of aftershocks cannot therefore be solely controlled by afterslip at depth. Also, stress loading of the

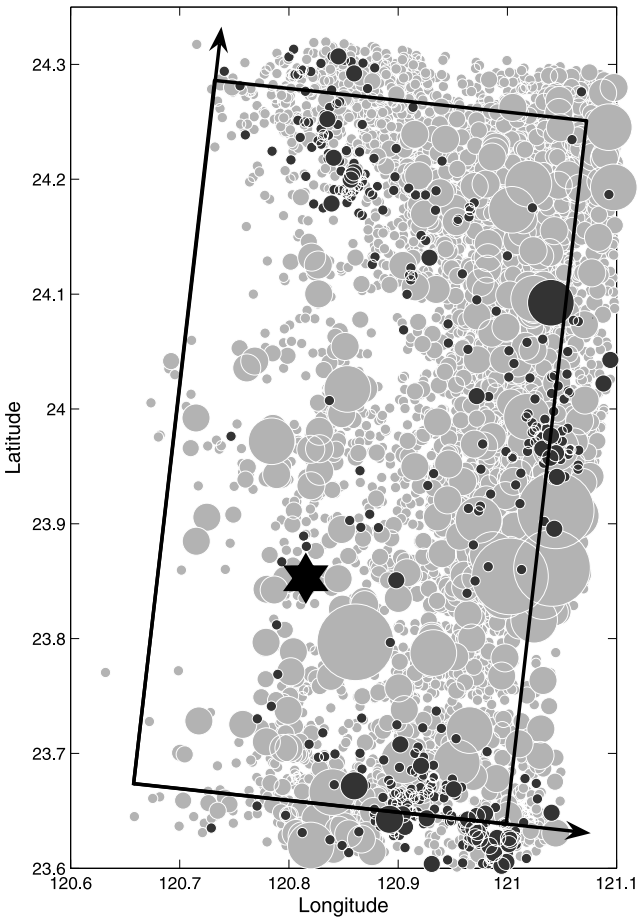

Figure 6. Map view of the M2.2+ on-fault seismicity in the 5 years before (black) and the 4 years after Chi-Chi (gray). Only the earthquakes within 5 km of the fault are considered. Hypocenter of the Chi-Chi earthquake is shown with the star.

ruptured fault by afterslip taking place at depth can only trigger aftershocks where the coseismic unloading is weak or even negative (i.e., coseismic loading). This mechanism therefore requires significant amounts of coseismic stress change variability on the main fault.

[31] Stress heterogeneity caused by slip spatial variability on the Chelungpu fault is expected to be strong. It is thus a likely candidate for explaining the vigorous aftershock activity. Applying the method of section 2, we try here to measure this heterogeneity. However, this estimation is a rather delicate issue, as a broad continuum of solutions can fit the data equally well. Model parameters $\{\bar{\tau}, \sigma_\tau, t_a\}$ can therefore only be bounded to lie within semi-infinite intervals, as is now detailed.

[32] Figures 7a and 7b show the earthquake rate density for the 5 years before and 4 years after Chi-Chi, respectively. The projection is done over an ~80-km long fault segment striking N3°E (see map in Figure 6) and using the vertical cross section of *Loevenbruck et al.* [2004]. Earthquakes within 5 km of this fault are considered. Preseismicity rates are very stable over the 5 years preceding Chi-Chi. Five seismicity clusters with size roughly ranging between 10 to 20 km can be identified, and we analyze them separately. Cluster 2 contains the hypocenter of the Chi-Chi earthquake.

[33] For each cluster, we reconstruct the evolution of the rate of M2+ earthquakes. Immediately after the main shock, the completeness magnitude goes up because of the extreme emissivity of the fault zone. This prevents a well-constrained analysis of the change in activity at early times (hours to days) after Chi-Chi; rate-and-state friction modeling makes predictions for these timescales, which potentially provide strong constraints on the stress variability. In the case of unsignificant variability $\sigma_\tau \ll |\bar{\tau}|$, the rate is expected to be constant until time $t_{\min} = t_a e^{-\bar{\tau}}$ is reached, and then decay as $\mu t_a/t$. If μ is well constrained, this regime of constant rate allows to estimate both $\bar{\tau}$ and t_a. If on the contrary $t_{\min}$ cannot be resolved because of a temporary high completeness magnitude, then, even in the case $\sigma_\tau \ll |\bar{\tau}|$, estimation of

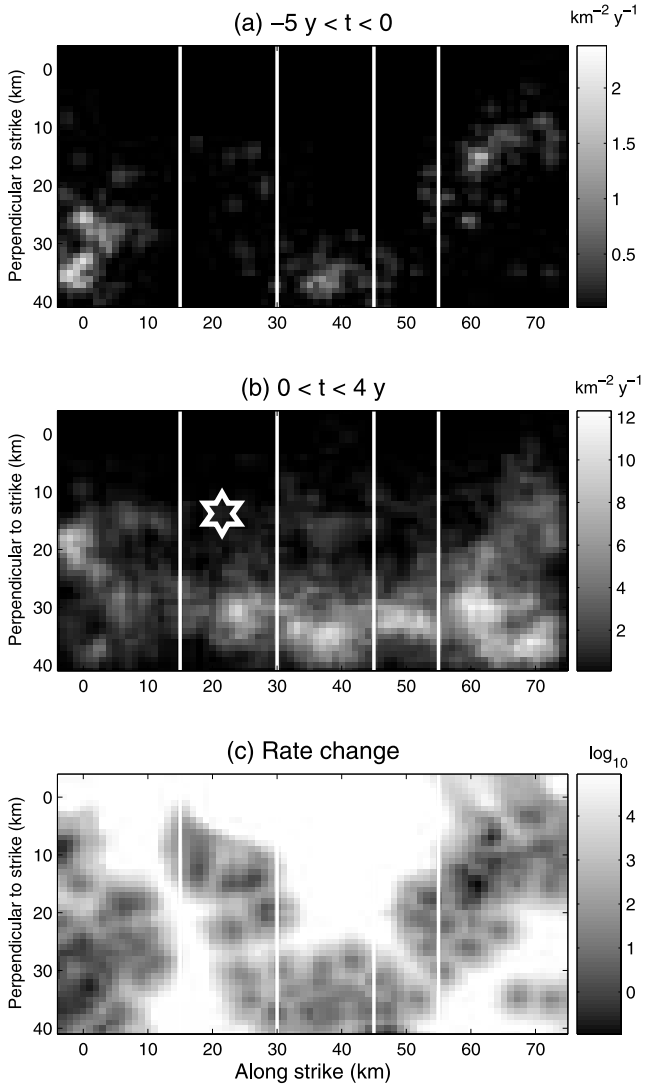

Figure 7. M2.2+ on-fault seismicity in (a) the 5 years before and (b) the 4 years after Chi-Chi, projected on the main fault. Hypocenter of the Chi-Chi earthquake is shown with the star. (c) Log_{10} of the rate change. We distinguish five clusters of activity, as separated by the vertical white lines. Along-strike coordinate increases toward north.

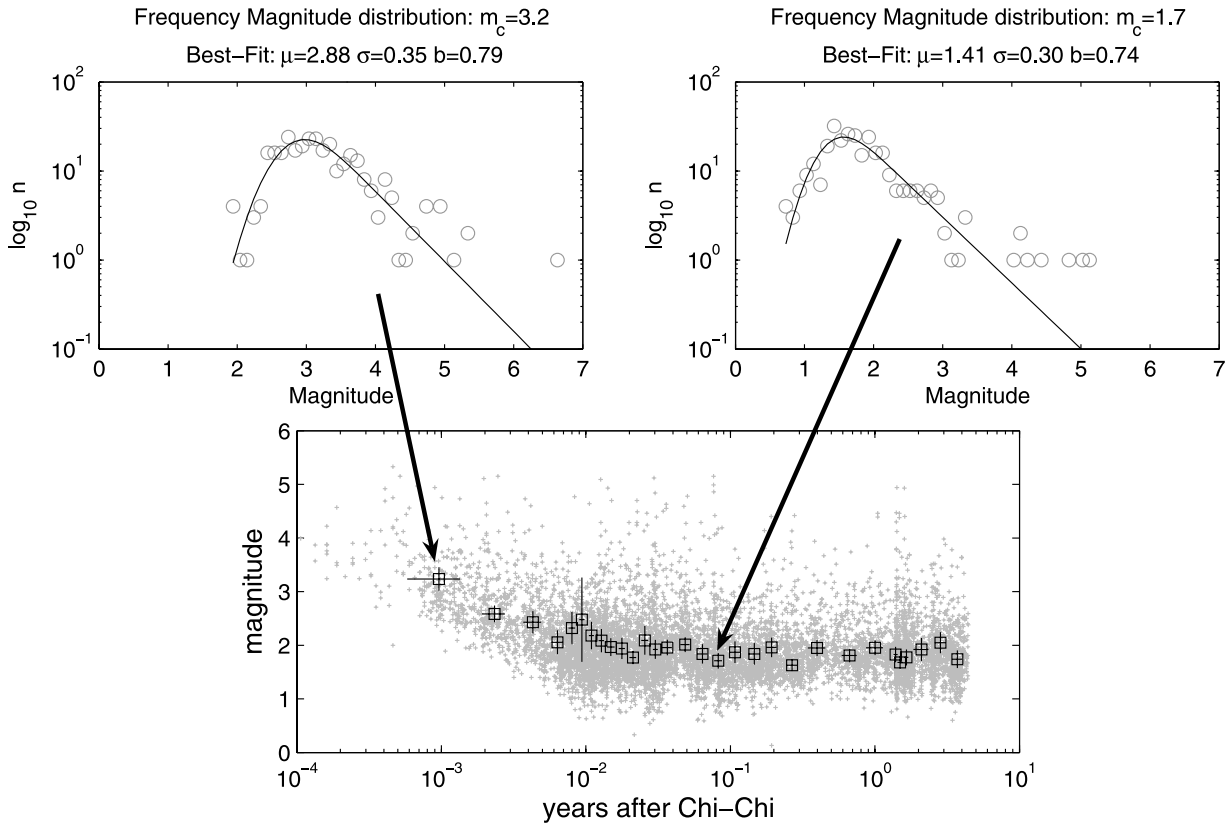

Figure 8. (Bottom) Magnitude cut-off, $m_c = \mu + \sigma$ versus time after Chi-Chi, for cluster 1 of Figure 7, with squares. The magnitudes and occurrence times of all the earthquakes are plotted with gray dots. Each square corresponds to 300 consecutive earthquakes. (Top) Two examples of how μ and σ are estimated by fitting the frequency-magnitude curve with the $\lambda_{\rm obs} = \lambda \times q$ model, where q is parameterized by both μ and σ, cf. equation (11).

$\bar{\tau}$ and t_a rely on long timescale behavior, i.e., the total number of triggered earthquakes, which here is not a resolved quantity since only 4.3 years of aftershocks were available for this study. It is therefore of primary importance to correctly estimate the seismicity rates as early as possible in the aftershock sequence.

[34] To do so, we adopt the approach detailed by *Ogata and Katsura* [1993] and estimate how many $M2+$ earthquakes are missed in the catalogue, therefore reconstructing the actual seismicity rates at early times. Note that the choice of $m = 2$ as a threshold is arbitrary here; it was made so because the uncertainty associated with the rate estimate is low at this magnitude.

[35] The observed rate of earthquakes of magnitude m at time t is $\lambda_{\rm obs}(t,m) = \lambda(t,m)\, q(m|\mu_t,\sigma_t)$ where $\lambda(t,m) = f(t)e^{-\beta m}$ follows the Gutenberg-Richter law with exponent β times some function $f(t)$ of time, to be estimated. The function q models the probability that the seismic network detects a magnitude m at time t and is taken to be of the form

$$q(m|\mu,\sigma) = \int_{-\infty}^{m} dm' \, \frac{1}{\sqrt{2\pi}\sigma} e^{-(m'-\mu)^2/2\sigma^2} = \frac{1}{2} + \frac{1}{2}\,\mathrm{erf}\left(\frac{m-\mu}{\sqrt{2}\sigma}\right) \quad (11)$$

Parameter μ gives the magnitude at 50% detection, while $\mu + \sigma$ can be seen as the equivalent of the usual magnitude of completeness m_c. This choice of q gives very good fits to the data. Also, the results are very stable to changes in the duration of observation. A second function q was tested, $q(m|\mu,\sigma) = \frac{1}{2\sigma}\int_{-\infty}^{m} dm'\, e^{-|m'-\mu|/\sigma}$, but was found to fit the data with less accuracy.

[36] Following Chi-Chi, consecutive sets of $N = 300$ earthquakes are independently considered for each of the five clusters. We use this value of N as a trade-off between small values (hence large uncertainties on μ and σ) and too large a value (hence assuming a constant detection function q over long time intervals during which it actually changes significantly). For each subset of earthquakes, parameters μ and σ of q and parameter β of λ are inverted, and their error covariance matrix is estimated. As an illustration, Figure 8 shows the fit for two such subsets for the first cluster (southernmost end of the rupture) along with m_c defined as $m_c = \mu + \sigma$ function of time. This m_c gives the magnitude such that the probability that the network detects an event with $m \geq m_c$ is >84%.

[37] Using this detection model and parameterization, we can correct for the changes in detectability with time and eventually invert the stress heterogeneity (namely, parameter σ_τ) for cluster 1. Figure 9 shows the uncorrected and corrected aftershock rates for the 4 years after Chi-Chi in

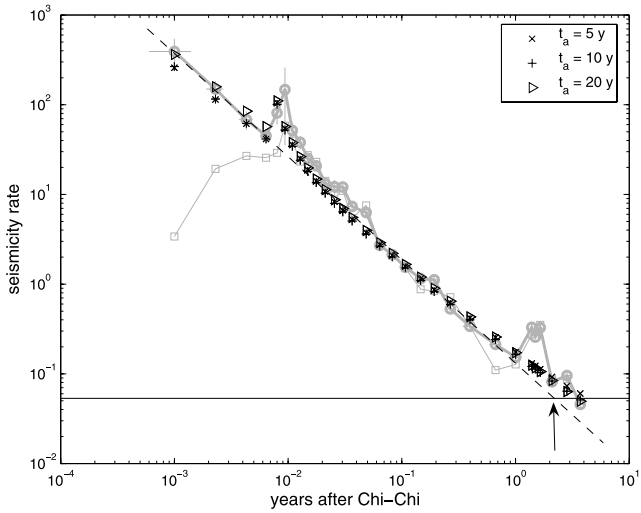

Figure 9. Seismicity rate in 1/day after Chi-Chi in the first on-fault cluster (between 0 and 20 km along strike, see Figure 7), uncorrected (gray squares) and corrected (thick gray circles) to account for the aftershocks missed in the first few days after the main shock. Only the magnitude band [2.0, 2.1] is considered. Both rates decay to the background rate (horizontal black line), defined as the rate in the 5 years prior to Chi-Chi. In black, best fits by a model with two triggers (at $t = 0$ and $t = 0.0065$ year after Chi-Chi) with variable stress steps, for three values of parameter t_a: 5, 10, and 20 years. All three models fit equally well the (corrected) data, given the error bars of the latter. Only the model with $t_a = 20$ years gives a negative $\bar{\tau}$ for Chi-Chi. Similarly good fits can be obtained for any value of t_a as long as $t_a > 4$ years; see text. For comparison, a simple estimation of t_a as being the time at which the extrapolated decay crosses the background rate is $t_a \simeq 2$ years (dashed line and arrow). The dashed line has $p \simeq 1.1$.

cluster 1, for the [2.0, 2.1] magnitude band. The correction is done to account for the earthquakes missed at short timescales, namely we infer λ from λ_{obs} given the parameters μ, σ, and β. These corrections are only significant at times less than about 4 days for this magnitude band. The maximum corrected rate, obtained at time $t \simeq 10^{-3}$ years, imposes that $t_a > 4$ years. A smaller t_a would imply initial rates significantly less than the corrected rates. At time $t \simeq 0.0065$ year, an abrupt increase in rate is observed. We therefore model the seismicity in cluster 1 as resulting from two triggers, one corresponding to Chi-Chi at $t = 0$, the second at $t = 0.0065$ year. The overall decay of the rate in this cluster is characterized by a p value larger than 1 ($p \simeq 1.15$); this value cannot a priori be accounted for by the model, which imposes p to be less than 1. However, the introduction of the second trigger at $t = 0.0065$ year allows for a good fit of the data, this second trigger causing the apparent p value to become larger than 1.

[38] Remarkably, Figure 9 shows that, as long as $t_a > 4$ years, there always exists a set of stress parameters such that the model can fit the data. Parameter t_a is therefore largely unconstrained, as are the stress parameters. If we further constrain the model by only admitting solutions for which Chi-Chi caused a negative mean stress change, i.e., an effective stress drop on the main fault, then t_a must be greater than about 12 years. Indeed, *Zhang et al.* [2003] found an average static-stress drop of the order of 5 to 10 MPa for this part of the fault (cf. their Figure 8a). Similarly, *Huang et al.* [2001] obtained 6.5 MPa for the southernmost 30 km. It is difficult to use those static-stress drop values for constraining parameter $\bar{\tau} = \frac{\text{static stress drop}}{A\sigma}$, since the value of $A\sigma$ is not well known. However, values ranging between $\bar{\tau} = -10$ to -100 can be expected to be realistic. Taking $\bar{\tau} < -10$, we obtain that $t_a > 14$ years. This estimate differs from a simple fit with one trigger at $t = 0$ and no stress variability, for which a $1/t$ law would cross the background rate at about 2 years; see Figure 9.

[39] Although all stress parameters are badly constrained, lower bounds on the standard deviation σ_τ of the stress changes caused by Chi-Chi on cluster 1 can be obtained, depending on t_a. For low (4 to 6 years) values of t_a, the mean stress change due to Chi-Chi is very large and positive, and the standard deviation must be small, cf. case A of Figure 2. This interval of t_a is not realistic, as it implies a coseismic stress loading of this portion of the fault. As t_a is increased, higher values of σ_τ at least of the order of $\bar{\tau}$ are needed, cf. case C of Figure 2. For $t_a > 14$ years, hence a realistic coseismic unloading of the fault, very high stress variability is expected, i.e., $\sigma_\tau \gg |\bar{\tau}|$. More precise inversion of σ_τ would require longer observation of the aftershock sequence, so to probe the right end part of the decaying curve.

[40] The overall decay shown in Figure 9 is characterized by $p \simeq 1.1$. Such a p value cannot a priori be reproduced by the model, which limits p to be less than 1. However, adding the second trigger at $t = 0.0065$ year allows for the slope to be locally greater than 1. Further work is needed to see if local triggering by aftershocks can indeed yield $p > 1$ for the overall decay. *Helmstetter and Sornette* [2002] showed that, for the (linear) epidemic-type aftershock sequence (ETAS) model, the overall ("dressed") p value can change at early times from the individual ("bare") one because of cascade triggering. However, p must be greater than 1 for the ETAS model to be stable, so that this short timescale regime is therefore predicted with $p < 1$. This is quite contrary to the present model, for which the "bare" p is less (or equal to) than 1, and one would like to know if a "dressed" value could become larger than 1. The ETAS model can be modified by adding a cut-off at $t = t_a$, similarly to the rate-and-state model. In this case, this model becomes stable even with $p < 1$. The change at short timescale to $p > 1$ could then explain our observation. *Ziv and Rubin* [2003] have performed simulations of a fault governed by rate-and-state friction where aftershocks can trigger their own aftershocks. Since no (subscale) stress variability was assumed, only $p = 1$ was obtained, similarly to the case of a single main shock [*Dieterich*, 1994]. *Marsan* [2006] proposed a cascade model using rate-and-state with stress variability, but its oversimplifying hypotheses would need to be reexamined.

[41] For the four other clusters, we summarize in Table 2 the lower bounds on t_a so (1) to fit the data with no constrain on $\bar{\tau}$, and (2) to fit the data, given a negative $\bar{\tau}$ (coseismic unloading of the fault). Values of σ_τ are very high (always greater than 80, still in units of $A\sigma$) in the latter case. *Hwang et al.* [2001] found that the stress drop was $\simeq$10 MPa larger in the north compared with the south of the

Table 2. Range of Possible t_a Values for the Five Clusters of the Chelungpu Fault Following Chi-Chi[a]

Cluster	$\widehat{t_a}$, years
1	>4
	>12
2	>10
	>12
3	>10
	>15
4	>12
	>23
5	>10
	>27

[a]The first lower bound on t_a is required to fit the local aftershock decaying rate with no condition on the sign of $\bar{\tau}$, while the second is conditioned so that the fault is unloaded by the main shock, i.e., $\bar{\tau} < 0$. The stress variability σ_τ increases with the value of t_a.

rupture. Also, *Huang et al.* [2001] proposed that the stress drop increased northward from 6.5 to >30 MPa. For a constant $A\sigma$ along the rupture, this would imply that t_a must be significantly greater than the largest lower bound given in Table 2 for the northernmost clusters (i.e., clusters 4 and 5). Parameter σ_τ must therefore be higher there than in the south. This shows that stress heterogeneity on the main fault is likely to vary in significant proportion along the fault.

4. Off-Fault Stress Heterogeneity

[42] As one goes away from the main fault, the triggering caused by Chi-Chi becomes less striking. Compared to the main fault (Section 3.2), other triggers become increasingly significant in controlling the local seismicity. This implies that (1) the rates in the 5 years prior to Chi-Chi are generally not stationary anymore and that (2) the model parameter set can become much larger, since each extra trigger is characterized by two parameters. This makes the inversion more difficult. However, since this inversion is now done on the full 9+ years of seismicity (1995–2004), parameter t_a is better constrained. This allows for a meaningful and relatively robust estimation of the stress parameters. We now detail this analysis by first focusing on the four seismicity shadows pointed out by *Ma et al.* [2005].

4.1. Triggering at Nansan

[43] At Nansan, *Ma et al.* [2005] found a strong quiescence, with a rate change of the order of or less than 10^{-1} in the 3–53 months following Chi-Chi, after an initial episode of triggering. The aftershock decay for magnitude $m \geq 2$ earthquakes in this area roughly follows a $1/t$ Omori's law but with some anomalous strong triggering until about 9 days after Chi-Chi (Figure 10a). This is best seen when plotting the cumulative number of aftershocks versus logarithm of time, as is done in Figure 10b; an Omori decay with $p = 1$ translates into a linear growth using this log scale. It took about 3 days for the seismic network to get back to completeness at $m \geq 2$.

[44] The rate-and-state model was fitted to these data. The parameter t_a was optimally set to 2 years. We discuss in section 4.1.1 how this choice was made. We first fit the time series from $t = -5$ years to $t = 0^-$ (just before the occurrence of Chi-Chi) with a background rate $\mu = 22$ year^{-1} and two triggers at $t = -2.81$ years and $t = -1.33$ years; see Figure 10c. The fit is very good.

[45] This model is then extrapolated to $t \geq 0$, yielding the seismicity rate that could have been expected had nothing special happened at $t = 0$ (dashed line, Figure 10c). The cumulative extra seismicity generated on top of this extrapolated seismicity is shown in Figure 10b, dashed line. It follows the initial triggering pattern described above (anomalously strong triggering up to 9 days, then an Omori-like decay) up to about 3 months. It then undergoes two consecutive dips, at $\simeq$3 and 14 months. Between those two dates, the extra seismicity increases slowly with time, indicating a mild triggering phase. Then at $t > 14$ months, a clear quiescence is observed, as already suggested in the analysis by *Ma et al.* [2005]. A precise assessment of the significance of the changes in seismicity rate is performed by perturbing the rate-and-state model with the two triggers prior to Chi-Chi and comparing the predicted and observed rate distributions for the two time intervals 0.16 year $< t <$ 1.16 years and 1.16 years $< t <$ 4.3 years; see Figure 11. The significance of the rate changes is very high for both time intervals; there is only a $10^{-4.9}$ and $10^{-4.5}$ chance, respectively, that such rate changes could have happened by chance, in the null hypothesis of no actual changes in the seismogenic process (see section 2.5). These changes correspond to seismicity rates that are roughly doubled and halved compared to the predicted rates. This indicates an abrupt and very significant change from triggering to quiescence at about 14 months after Chi-Chi.

[46] We fitted the whole seismicity time series from $t = -5$ years to $t = +4.3$ years (i.e., from September 1995 to February 2004), excluding the first 9 days after Chi-Chi. The strong triggering observed during this 9-day period cannot be reproduced by the model. Some of this seismicity is possibly due to dynamic triggering and is therefore beyond the scope of the present model based on static-stress steps. We added three more triggers to the two previous ones at $t = -2.81$ years and $t = -1.33$ years, (1) at $t = 0$ (Chi-Chi), (2) at $t = 0.16$ year, and (3) at $t = 1.16$ years. The trigger at $t = 0.16$ year was initially set at $t = 3$ months ($t = 0.25$ year) on the basis of Figure 10b but was eventually readjusted to $t = 0.16$ year as the fit to the data is then maximized. The last trigger at $t = 1.16$ years corresponds to the start of the quiescence, 14 months after Chi-Chi.

[47] Again, the fit is very good. The model mimics the initial triggering phase and the two relatively abrupt changes. The goodness of fit is better shown in Figure 10d, where the cumulative number of earthquakes is plotted against the operational time $\Lambda(t) = \int_{-5 \text{ years}}^{t} ds\ \lambda(s)$. Apart from the 9-day gap immediately after Chi-Chi, the plot is very close to linear, as expected for a good model. Table 3 details the stress distributions (means and standard deviations, along with their uncertainties; see below) found by inversion. The last two triggers have negative means and significant variability, hence causing the seismicity to temporarily increase and eventually drop, as observed in the data.

[48] The remarkable results are that the model with five triggers (1) can well explain the 9+ yearlong seismicity time series, and (2) suggests that the late quiescence starting

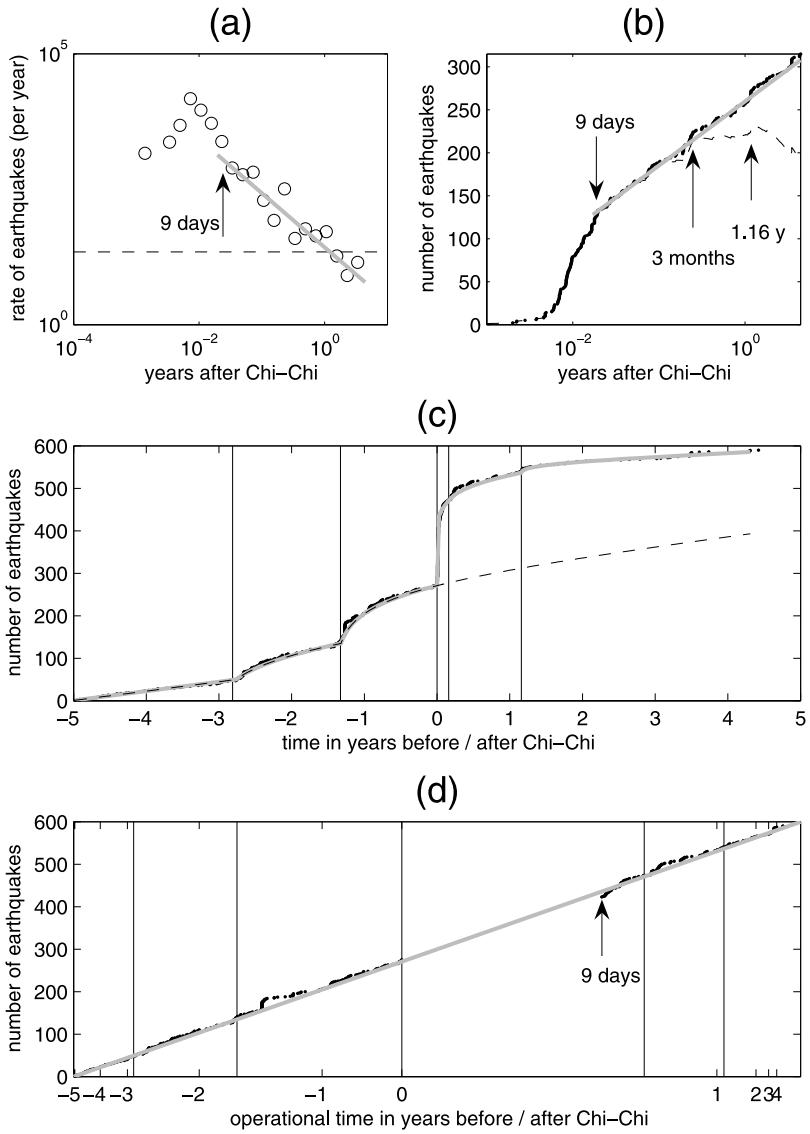

Figure 10. Observed and modeled $M2+$ seismicity at Nansan, from September 1995 to February 2004. (a) Rate of earthquakes per year after Chi-Chi. The dashed line is the background rate $\mu = 22$ per year. An Omori-like decay in $1/t$ is indicated by the gray line. At $t < 9$ days, anomalously strong triggering compared to this decay is observed. (b) Cumulative number of earthquakes after Chi-Chi. The gray line in $\sim\log t$ is similar to an Omori decay. Dashed line, extrapolated activity, as predicted by the model fitted to $t < 0^-$, minus the actual seismicity. This equals the extra seismicity observed on top of what is predicted, had Chi-Chi not occurred. (c) Seismicity time series compared to the best model (gray line) with five triggers as indicated by the vertical lines. The extrapolation used in (b) is shown in dashed line. (d) Seismicity versus operational time in years; see text. Gray line, best model. This model is not fit during $0 < t < 9$ days because of the anomalously strong triggering taking place during this period.

14 months after Chi-Chi is not directly caused by the main shock itself but rather by latter modifications of the state of stress in Nansan. The distribution of the stress change due to Chi-Chi alone is found to be homogeneous, with positive stress value $\bar{\tau} = 2.42 \pm 0.24$ and practically no heterogeneity; see Table 3. We further develop those two results.

4.1.1. Quality and Uniqueness of the Model and Parameter Uncertainties

[49] A set θ of 11 parameters is inverted to fit the whole time series (t_a and the mean and standard deviation of the Gaussian stress distributions for each of the five triggers). As mentioned in section 2, the full covariance matrix of the error on the parameters is computed by least squares fitting J close to its minimum. An important question is whether the best parameter set $\hat{\theta}$ is the only acceptable one or if other significantly different sets could also fit the data nearly equally well. This is explored by randomly and significantly perturbing $\hat{\theta}$ and by estimating the marginal laws for each component θ_i of θ. For all the parameters, the marginal laws are Gaussian in shape with relatively narrow widths. We could not find any other, significantly different acceptable solution that would appear as a second peak in those

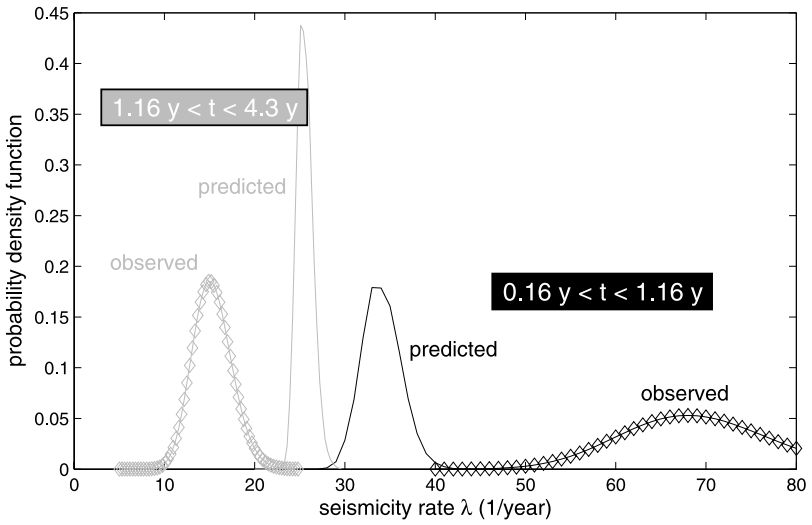

Figure 11. Seismicity rate distributions for the Nansan region and *M*2+ earthquakes, for two time intervals: 0.16 year < t < 1.16 years and 1.16 years < t < 4.3 year after Chi-Chi. The predicted rates are obtained by perturbing the best model parameters, cf. section 2.

marginal laws. We therefore conclude that the obtained minimum of J provides the overall best fit to the data and excludes the existence of other significantly different solutions (i.e., acceptable solutions outside the error range on the parameter provided by the error covariance matrix). Note that parameter t_a is well constrained (its error is Δt_a = 0.55 year), which gives us confidence in our results as this parameter is of great importance in this method; see section 2.4.

[50] The robustness of the model is further tested by varying the number of triggers from three to five, keeping the first three triggers at times t = −2.81 years, t = −1.33 years, and t = 0 (Chi-Chi), and adding zero, one, or two triggers at t = 0.16 year and t = 1.16 years. To compare these four models, the Akaike Information Criterion AIC = 2N + 2 min J is used [*Akaike*, 1973], where N is the number of free parameters. With this criterion, adding one trigger, hence two parameters, is considered as a significant progress only if the best cost value min J is decreased by at least two units. Table 3 details the results. Adding trigger 5 strongly improves the model (ΔAIC = −22.4) more than adding trigger 4 (ΔAIC = −11.0). Adding trigger 4 on top of trigger 5 only slightly improves the model (ΔAIC = −23.8 + 22.4 = −1.4). This implies that trigger 5 is an important contribution in the model, while we could remove trigger 4 at not too high a cost. Most importantly, a model with only two triggers before Chi-Chi plus Chi-Chi itself cannot explain the observed quiescence developing after about 14 months after Chi-Chi. The two dips in the extra seismicity seen on Figure 10b are sharp and significant (cf. Figure 11) and are in both cases preceded by a short triggering phase. These features cannot be reproduced with only those three triggers, and two extra triggers at t = 0.16 year and t = 1.16 years are needed to account for these features.

[51] Finally, with the notable exception of the model with triggers 1 to 4 (i.e., excluding trigger 5), the t_a parameter is found to be stable from one model to the other, and the $\bar{\tau}$ and σ_τ parameters for the first three triggers too. This strengthens our confidence that the model has captured the important features in the time series and is able to reproduce them.

Table 3. Model Parameters for the Four Tested Models, Along With Their Minimum Value of the Cost Function Min J and Aikake Information Criterion AIC[a]

Trigger	$\widehat{t_a}$ = 1.88 ± 0.55 years	$\widehat{t_a}$ = 1.5 years	$\widehat{t_a}$ = 15 years	$\widehat{t_a}$ = 2 years
1	1.73 ± 0.29	1.95	−0.16	1.82
	0 ± 0.89	0	2.16	0
2	2.55 ± 0.55	3.03	−0.53	2.69
	0.53 ± 1.02	0	3.08	0
3	2.42 ± 0.24	2.76	2.04	2.43
	0 ± 0.46	0	0.02	0
4	-0.87 ± 0.80	NA	−5.44	NA
	1.89 ± 0.70		4.48	
5	−4.25 ± 1.86	NA		−4.52
	5.14 ± 1.70			5.12
Min J	−1495.9	−1468.1	−1481.1	−1492.5
AIC = Min J + N	−1484.9	−1461.1	−1472.1	−1483.5

[a]For the five triggers, the mean $\bar{\tau}$ (top) and standard deviation σ_τ (bottom) of the distribution of the stress step are given, unless the trigger is not considered by the particular model (NA). Estimation of the uncertainties is also given for the full model with all the five triggers.

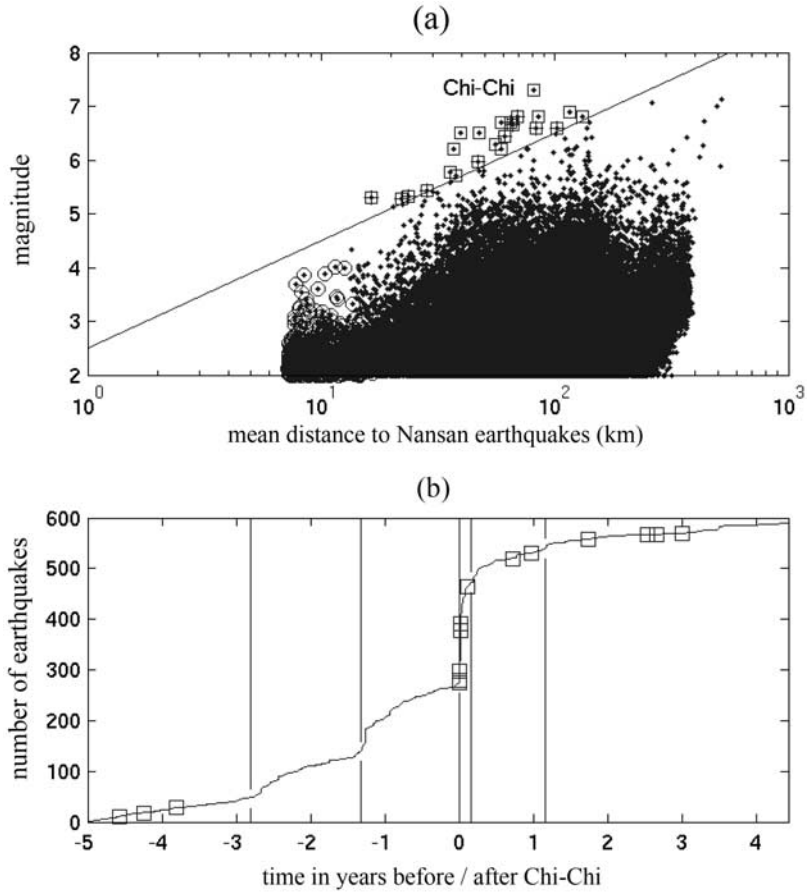

Figure 12. (a) Magnitude m versus mean distance r to the $M2+$ Nansan earthquakes for all the $M2+$ earthquakes in the catalogue and time interval under study. The line gives the position of all earthquakes that create identical stresses as in equation (12). All 25 earthquakes above this line are shown with squares. Those that occur in the first 9 days after Chi-Chi are indicated with crosses (+). Chi-Chi earthquake is the event that caused the largest stress. ''Internal'' earthquakes that occurred in Nansan region are indicated with circles (○). (b) Earthquake time series in Nansan, with the occurrence times of the 25 earthquakes selected in Figure 12a shown with squares. Note that many earthquakes occurred just after Chi-Chi, so that some boxes are actually multiple.

4.1.2. Quiescence not Directly Caused by Chi-Chi

[52] The four tested models (i.e., with three to five triggers) all indicate that the Chi-Chi earthquake, here modeled as trigger 3, created a stress step distribution with almost no variance and a positive mean. The best model with five triggers yields a mean $\bar{\tau}$ equal to 2.42 ± 0.23 for trigger 3. Therefore according to our working hypotheses, Chi-Chi could only promote triggering and is not the direct cause of the quiescence observed to start 14 months after it.

[53] This quiescence is well explained by trigger 5. As already noted, the onset of this quiescence is relatively sharp (Figures 10b and 10c). This strongly suggests that its cause did occur suddenly. Also, an ≃7-day period of triggering is seen immediately after this time, during which eight $M2+$ earthquakes were triggered on top of the expected seismicity (as obtained by extrapolating the best model with only the first four triggers). Both observations point out to a sudden change in stress conditions at Nansan, i.e., implying a process which duration is of the order of or less than days. The initial triggering is well reproduced by trigger 5, which has a negative mean stress $\bar{\tau} = -4.25 \pm 0.77$ but a strong stress variability $\sigma_\tau = 5.14 \pm 0.60$.

[54] We investigate the nature of the two triggers before and two triggers after Chi-Chi. In particular, we ask the question as to whether those triggers are of seismic origin, i.e., whether there is a significantly large earthquake in the vicinity of this area around the time of the trigger that could have caused the stress change. To do so, we estimate an order of magnitude of the stress change $\Delta\sigma_i$ over the Nansan region caused by earthquake i as

$$\Delta\sigma_i \sim 10^{1.5\, m_i}\, r_i^{-3} \tag{12}$$

where m_i and r_i are the magnitude and mean distance to all $M2+$ earthquakes in Nansan that occurred during the 9+ years under study for earthquake i. In Figure 12a, we plot m_i versus r_i for all $M2+$ earthquakes in the catalogue. Isostress lines are parallel to each other on this plot. The largest stress was caused by Chi-Chi, as expected from the seismicity time series. We select the 25 largest stress values corresponding to the earthquakes above the isostress line as depicted on the graph. In the context of static-stress triggering, those 25 earthquakes are expected to be the most important

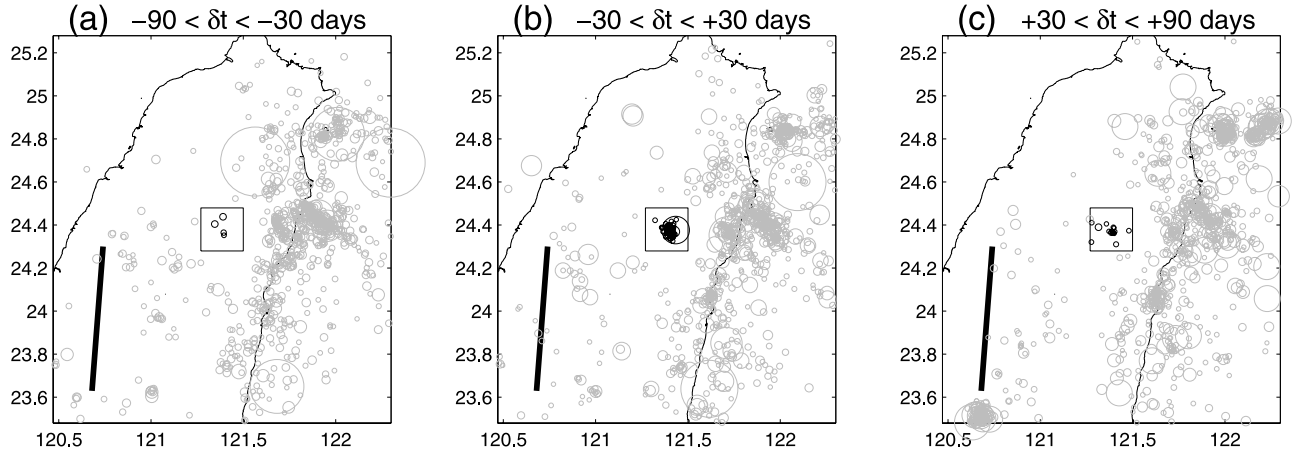

Figure 13. Locations of all the earthquakes in the catalogue that occurred around the time of the second trigger −1.33 years before Chi-Chi for three temporal windows. Parameter δt is the time difference between the earthquakes and the time of the second trigger. Circle size indicates the magnitude. The black straight line shows the main feature of the surface rupture of the Chi-Chi earthquake. The Nansan region is indicated with the box.

causes of seismicity changes. Figure 12b displays their occurrence times. Interestingly, the first, second, and fifth triggers do not coincide with any of those events.

[55] This however does not rule out the possibility that earthquakes which occurred inside the Nansan region could have caused these changes. Such ''internal'' earthquakes are shown with circles on Figure 12a. While their stresses as estimated by equation (12) are relatively low, their spatial clustering and errors in location imply that actual stresses could be much higher (see *Marsan* [2005] for more on this issue). We show in Figures 13 and 14 the seismicity around the times of the second and fifth triggers. At $\delta t = 0.06$ year ($\simeq$22 days) after the time of the second trigger, a M3.9 earthquake occurred within the region, as can be seen in Figure 13b. It contributed to, if not causing, the significant change in seismicity following trigger 2. For the first and fifth triggers, no similar seismic candidates can be found.

[56] This analysis suggests that the first and fifth triggers are either (1) earthquakes that caused stress changes in the Nansan region that are significantly greater than predicted by the static stress expected from the occurrence of a dislocation in an elastic halfspace [as roughly modeled by equation (12)], or that (2) they are not of seismic origin. In particular, the fifth trigger that we found to be the most likely cause of the observed quiescence does not seem to correspond to any significantly large earthquake. The quiescence could then be the consequence of a slow rupture or aseismic slip, as for example proposed by *Ogata et al.* [2003] in the case of the Landers sequence. We also noticed that this evolution of seismicity does not significantly change with depth, although the onset of the quiescence occurs later, at about $\simeq$2 years after Chi-Chi at shallow ($z < 8$ km) depth.

4.2. Triggering at Taichung

[57] West of the Chi-Chi rupture, off-coast seismicity was promoted for about 2 days immediately following the main shock. Because of a high magnitude of completeness taken here as $m_c = 2.75$, only a small number of earthquakes are considered in this region. A constant seismicity rate in time is found to be a suitable model for the 5 years that precede Chi-Chi; see Figure 15.

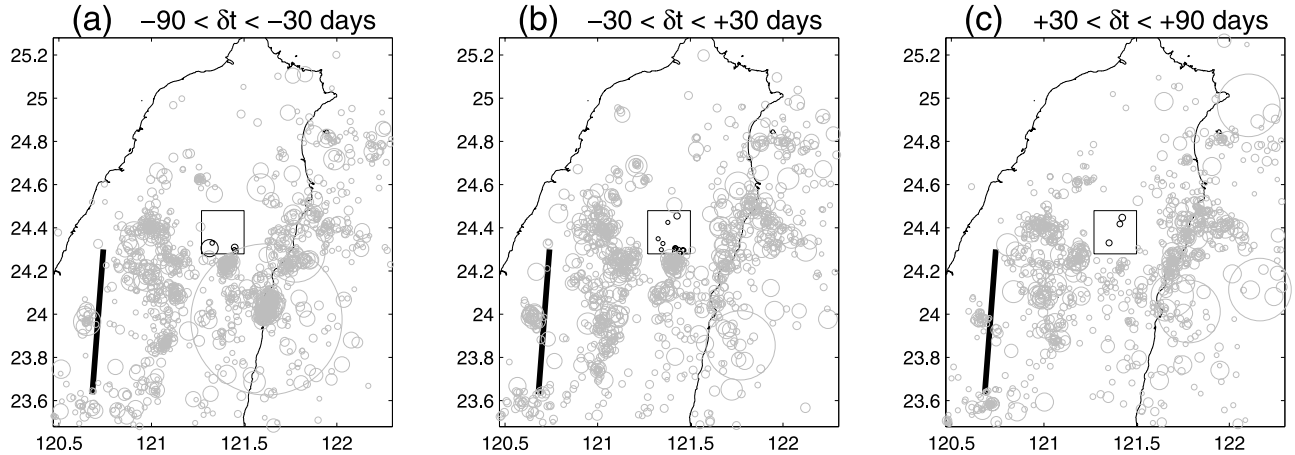

Figure 14. Same as in Figure 13, for the fifth trigger at 1.16 years after Chi-Chi.

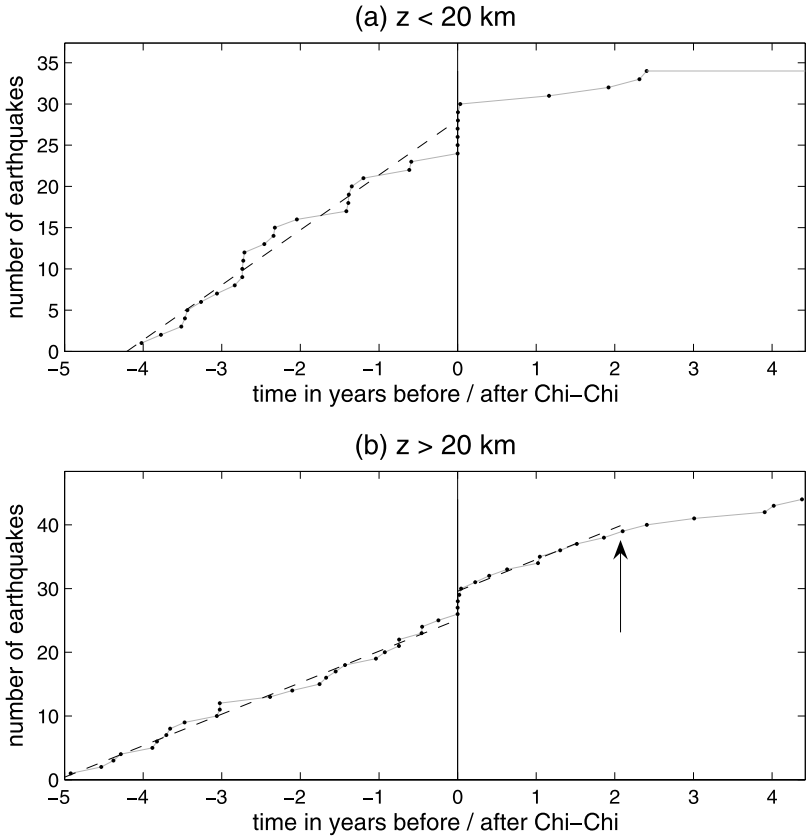

Figure 15. $M2.75+$ seismicity time series in the Taichung region, (a) at shallow depth $z < 20$ km and (b) at greater depth $z > 20$ km. In both cases, a constant seismicity rate is sufficient to explain the data before Chi-Chi (dashed line). After 2 days of initial triggering, a quiescence is seen at shallow depth (Figure 15a), while it is delayed by about 2 years at greater depth (Figure 12b).

[58] The behavior of post-Chi-Chi seismicity here strongly depends on depth. At shallow depth $z < 20$ km, a clear quiescence can be seen right after the 2 days of initial triggering. The significance of the change is high, with a probability $\mathcal{P} = 10^{-2.6}$ that it could happen by chance, as inferred from the probability densities of Figure 16a. Given the small number of earthquakes, we could not reliably estimate the variability of the stress change caused by Chi-Chi in this shallow region. Clearly, the mean stress must be negative.

[59] A different behavior is obtained at greater depth $z >$ 20 km. No quiescence is seen in the first 2 years after Chi-Chi, with a 99% significance level, cf. Figure 16b. A mild quiescence is then found, with a γ value of -1.45, starting 2 years after Chi-Chi. As with the Nansan region, the start of the quiescence at depth does not coincide with any significant large earthquake within or in the vicinity of this region.

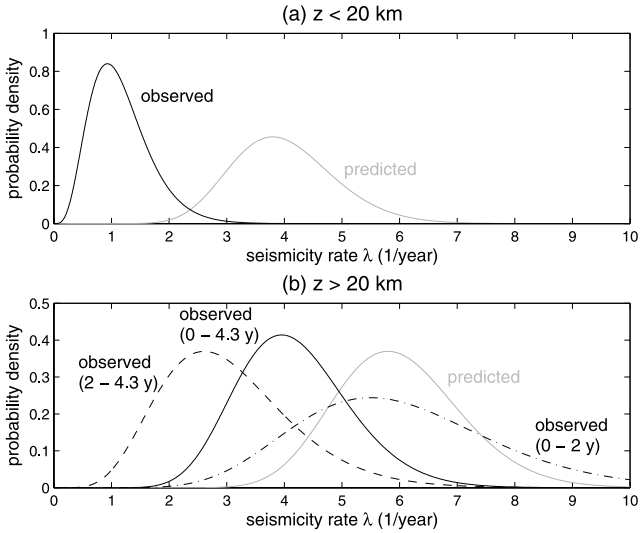

Figure 16. Probability density functions of the seismicity rate at Taichung, for (a) $z < 20$ km and in the time interval +2 days to +4.3 years after Chi-Chi, (b) $z > 20$ km and three time intervals +2 days to +4.3 years, +2 days to +2 years, and +2 years to +4.3 years. The predicted rate distribution is shown in gray and is obtained by perturbing the model (a constant rate in time). The probabilities that these changes in rate could happen by chance (cf. section 2.5) are (a) $10^{-2.6}$, (b) $10^{-0.97}$, $10^{-0.3}$, and $10^{-1.45}$, respectively.

4.3. Triggering at Kaoping

[60] The seismicity time series at Kaoping is complex and significantly depends on depth. Unlike the activity on the Chelungpu fault or at Nansan, the influence of Chi-Chi is difficult to isolate. Figures 17 and 18 show this seismicity at shallow and greater depth and at different timescales.

[61] For $z < 10$ km, there is no remarkable triggering but instead a slow deceleration of the activity, which start is not

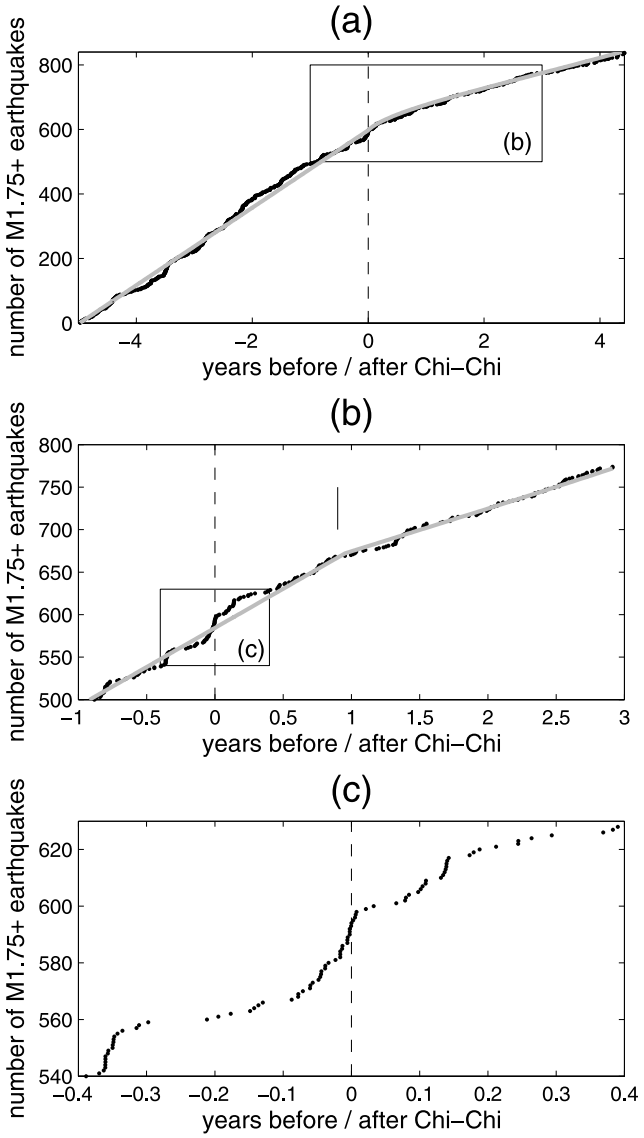

Figure 17. Seismicity in Kaoping at shallow depth ($z <$ 10 km), seen at three different timescales. Gray lines, model with parameters (a) $t_a = 3$ years, $\mu = 120$ year^{-1}, $\bar{\tau} = -3$, $\sigma_\tau = 3.2$, trigger at $t = 0$; (b) $t_a = 3$ years, $\mu = 92$ year^{-1}, $\bar{\tau} = -1.1$, $\sigma_\tau = 0.5$, trigger at $t = 0.9$ year (vertical mark).

well resolved. We here try to model the seismicity by imposing a trigger at the time of Chi-Chi ($t = 0$) and then by changing this occurrence time if the model is observed to be significantly improved by doing so. Unfortunately, the answer then depends on the duration of observation. At long timescales (Figure 17a), assuming a prior rate of $\mu =$ 120 year^{-1}, the seismicity can be fitted by Chi-Chi changing the stress with $\bar{\tau} = -3 \pm 0.6$, $\sigma_\tau = 3 \pm 0.5$, and $2 \leq t_a \leq$ 6 years. This implies some stress variability but not enough to significantly delay the quiescence.

[62] Looking at shorter timescales (Figure 17b), the seismicity can be modeled as a stationary Poisson process from $t = -1$ year to $t = 0.9$ year (vertical mark) with $\mu =$ 92 year^{-1}, and a trigger at $t = 0.9$ year characterized by $\bar{\tau} = -1.1 \pm 0.9$, $\sigma_\tau = 0.8 \pm 1$, and $t_a \geq 1$ year. Note that the uncertainties on the stress parameters are quite large. This can be caused by the timing of this trigger, which is not well constrained. In particular, unlike the fifth trigger in Nansan, there is no noticeable initial triggering phase that could help constraining it.

[63] At even shorter times (Figure 17c), it is difficult to see any influence of Chi-Chi on the local seismicity. These observations and modeling point out to the difficulty in explaining seismicity changes in remote locations in an unambiguous way. Here two very different models can be proposed that can correctly mimic the temporal pattern depending on what timescale is examined. The quiescence is observed to start at around $t = 0.9$ year after Chi-Chi at the intermediate timescale of Figure 17b; this is different from a quiescence caused by Chi-Chi and delayed because of stress heterogeneity, since there is no initial triggering phase during those $\simeq$11 months.

[64] At greater depth ($z > 10$ km), similar conclusions are obtained. At long timescales, there is a significant change in rate shortly after Chi-Chi and lasting for about 2 years; see Figure 18a. Assuming the simplest model, which is a prior stationary rate of $\mu = 211$ year^{-1}, this observation can be explained by Chi-Chi changing the stress according to $\bar{\tau} = -1.2 \pm 1$, $\sigma_\tau = 0.3 \pm 0.3$, and $0.4 \leq t_a \leq 2$ years. At shorter timescales (Figure 18b), the 4 years of seismicity can be modeled with one trigger at $t \simeq -0.84$ year, at which time a *M*5.5 occurred. Model parameters are then $\bar{\tau} = 0.5 \pm 0.3$, $\sigma_\tau = 3.6 \pm 0.4$ for this trigger, and $t_a \leq 0.5$ year. No significant change can then be related to the occurrence of Chi-Chi.

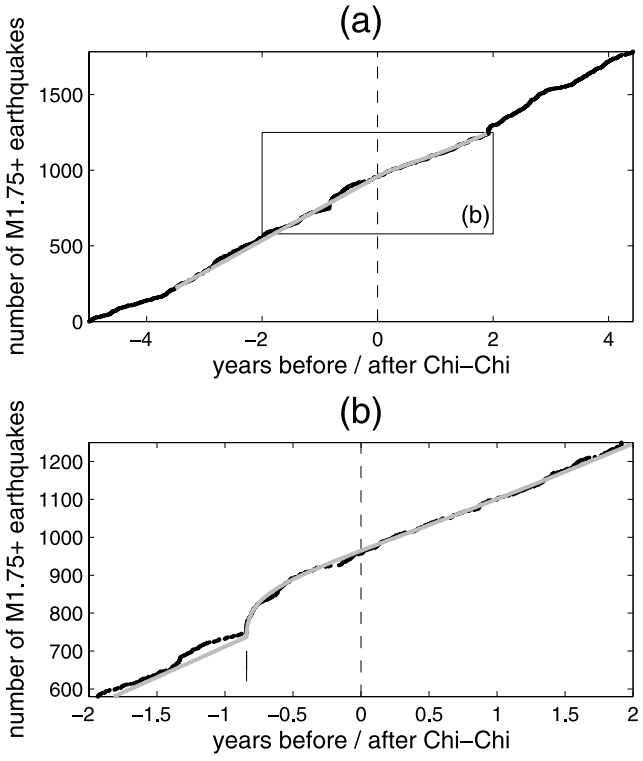

Figure 18. Same as Figure 17, at greater depth ($z > 10$ km). Gray lines, model with parameters (a) $t_a = 0.6$ year, $\mu =$ 211 year^{-1}, $\bar{\tau} = -1.2$, $\sigma_\tau = 0.3$, trigger at $t = 0$; (b) $t_a =$ 0.5 year, $\mu = 161$ year^{-1}, $\bar{\tau} = 0.5$, $\sigma_\tau = 3.6$, trigger at $t = -0.84$ year (vertical mark).

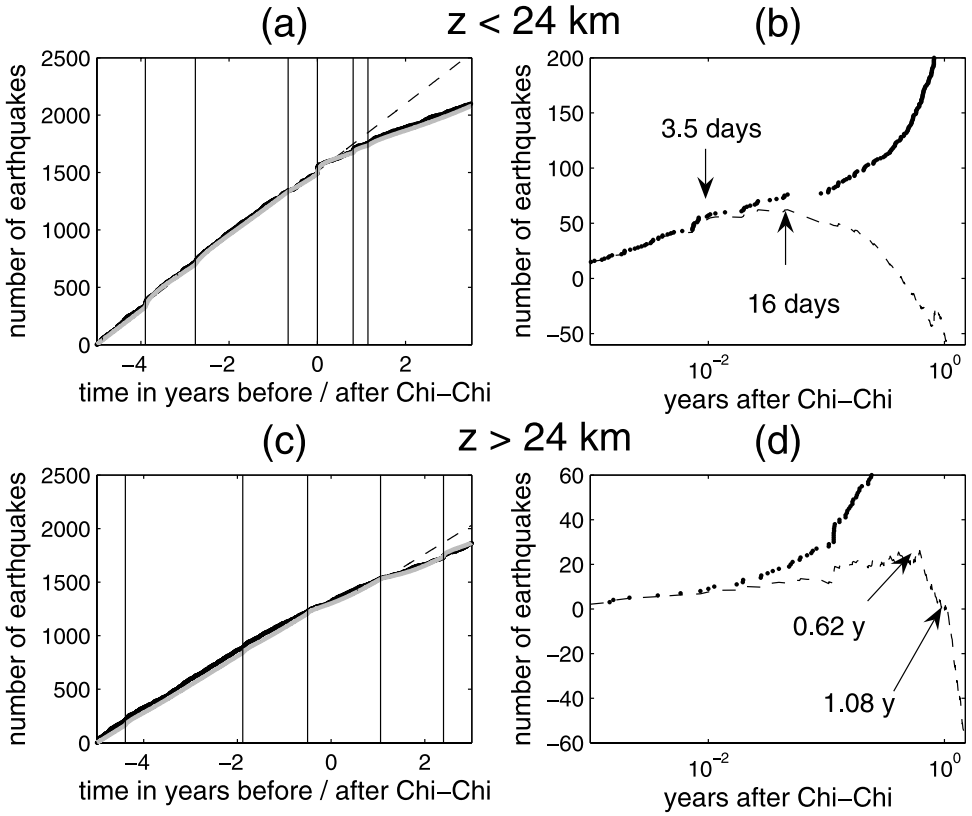

Figure 19. (a and c) Time series and (b and d) post-Chi-Chi seismicity for Huathung for the two depth intervals $z < 24$ km and $z > 24$ km. (a and c) $M2.25+$ seismicity in black, along with the predicted post-Chi-Chi activity in dashed line, and the best model (gray line) fitted over the whole time interval. (b and d) $M2.25+$ post-Chi-Chi seismicity (black dots) minus the predicted activity (dashed line).

[65] This study of the Kaoping region shows how ambiguous such an analysis can be when only slight fluctuations of the seismicity are observed around a mean behavior. There exists then a strong dependence on the scale of observation; the results are significantly different when considering either 9 or 4 years of activity. Firm conclusions on the role of Chi-Chi on the local faults cannot therefore be reached here.

4.4. Triggering at Huathung

[66] We divide the seismicity in the fourth region (Huathung) into a shallow $z < 24$ km and a deeper $z > 24$ km activity. The transition at 24 km corresponds to the median depth for the 9 years of seismicity studied. The completeness magnitude is at 2.25 for both subsets.

[67] The choice of triggers was done separately for the two depth intervals. We first select the dates with the most obvious changes in seismicity rates, and we then omit those triggers which inclusion did not decrease the AIC (cf. section 4.1.1). We ended up with six triggers for the shallow activity (time interval -5 years $< t < +3.5$ years) and five triggers for the deeper part (-5 years $< t < +3$ years); see Figure 19. Optimal values of t_a were found to be small, equal to 6 and 2 months only, for the shallow and deep sections, respectively.

[68] Only the shallow activity requires Chi-Chi to be a trigger, with a negative mean stress $\bar{\tau} = -4.14$ and high variability $\sigma_\tau = 6.10$. There, the predicted rate for $t > 0$ had Chi-Chi not occurred is clearly seen to be greater than the observed rate, although with a delay extending from 3.5 to 16 days (Figure 19). During these few days, triggering is observed. Chi-Chi is therefore found to have caused a delayed quiescence at shallow depth, with a very high significance level (probability $\mathcal{P} = 10^{-7.9}$ to occur by chance). Since the initial triggering phase is short (less than $\sim$2 weeks), it could alternately be explained by dynamic triggering activating a local, short-lived aftershock sequence. Such a mechanism has been suggested for the reactivation of the Yalova swarm in Turkey following the 1999 Duzce earthquake [*Daniel et al.*, 2006] and also for remotely triggered sequences in the Western United States [*Brodsky*, 2006]. The present model only accounts for static-stress changes, and therefore require high stress variability to explain both the initial triggering and the delayed quiescence.

[69] At greater depth, the main shock does not seem to trigger nor inhibit the activity. The time series is well fitted for the first 7.5 months by the extrapolated seismicity without requiring a trigger at the time of Chi-Chi (Figures 19c and 19d). Then, at 7.5 months after the main shock, a sudden rate decrease is seen, which is possibly not directly caused by Chi-Chi.

4.5. Other Zones

[70] We extended this analysis to all of Taiwan by systematically searching for quiescences, either immediate

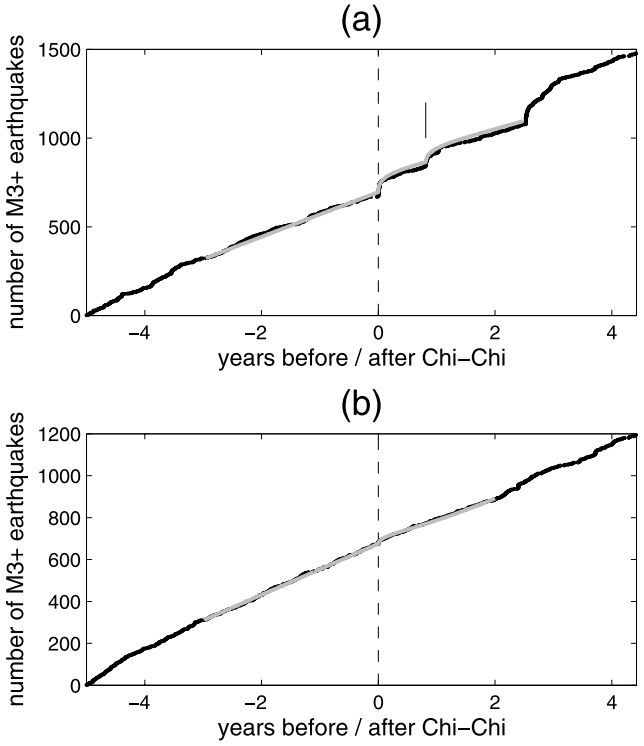

Figure 20. *M*3+ seismicity and best models for the forearc region 5 of Figure 5 for (a) $z < 20$ km and (b) $z > 20$ km. The gray lines are the best models, corresponding to parameters (a) $t_a = 0.6$ year, $\bar{\tau} = -0.3$, and $\sigma_\tau = 4.6$ for Chi-Chi trigger at $t = 0$ and $\bar{\tau} = 0.9$ and $\sigma_\tau = 3.3$ for the second trigger at $t = 0.813$ (vertical mark); (b) $t_a = 0.3$ year, $\bar{\tau} = -0.75$, and $\sigma_\tau = 3.5$ for trigger at $t = 0$.

or delayed, that could be related to Chi-Chi. The region was first divided into tectonic structures, and each of those subregions was examined individually. Two additional zones are found to experience a negative change in seismicity rate starting at the time of Chi-Chi. All other regions either show triggering or no significant change.

[71] In the forearc of the Ryukyu subduction (zone 5 in Figure 5), slip partitioning of the oblique convergence of the Philippine Sea plate and Eurasia is accommodated by trench-parallel strike-slip faulting. In this very seismically active area, delayed quiescence is observed following Chi-Chi. Figure 20 shows the *M*3+ seismicity time series, along with the best models, at shallow and greater depths. In both cases, the influence of Chi-Chi is characterized by a negative or zero $\bar{\tau}$ and significant amounts of stress variability. At $z < 20$ km, we find $\bar{\tau} = -0.3 \pm 0.8$ and $\sigma_\tau = 4.6 \pm 0.7$, while at $z > 20$ km, $\bar{\tau} = -0.75 \pm 0.6$ and $\sigma_\tau = 3.5 \pm 0.6$. In both cases, t_a is found to be less than 1 year. Such stress changes explain (1) the initial triggering, which is particularly clear at shallow depth, and (2) the relaxation to seismicity rates significantly lower than the expected rate, most particularly at depth.

[72] More to the north, zone 6 in Figure 5 also experienced a clear quiescence after Chi-Chi. This corresponds to the termination of the Okinawa Trough, a backarc extension basin, as well as deeper seismicity at the interface between the slab and the Eurasia plate. We again divide the seismicity according to depth. At shallow depth $z < 10$ km, which mostly correspond to normal faulting associated with the backarc opening, a very significant quiescence is observed, which can be modeled by Chi-Chi changing the stress according to $\bar{\tau} = -1 \pm 0.4$ and $\sigma_\tau = 0.2 \pm 3$. The stress variability is unfortunately badly constrained, mostly because of a locally large t_a (the best fit value being $\widehat{t_a} = 3$ years). At greater depth, the subduction earthquakes occur at almost stationary rate for 5 years including the occurrence of Chi-Chi. At $t = 0$, a slight change in rate can be modeled with $\bar{\tau} = -0.3 \pm 0.5$, $\sigma_\tau = 1.8 \pm 0.7$, and $0.2 \leq t_a \leq 0.8$ year, cf. Figure 21, hence a case of very mild triggering with rapid decay to background rate. It is somewhat remarkable that such an area distant by more than 100 km from the end of the Chi-Chi coseismic rupture and corresponding to a very different tectonic setting can exhibit such a clear shutting down of the seismicity. At shallow depth, this quiescence is almost immediate, very significant, and affects a large area ($\simeq$1000 km^2).

5. Discussion

[73] The rate-and-state model can explain the evolution of the seismicity in all the various regions examined, with the occasional exception of limited time intervals following the Chi-Chi earthquake when high rates of seismicity, possibly related to a phase of dynamic triggering and its subsequent aftershock sequence, are not reproduced by the model. The analysis becomes tedious as one looks away from the main

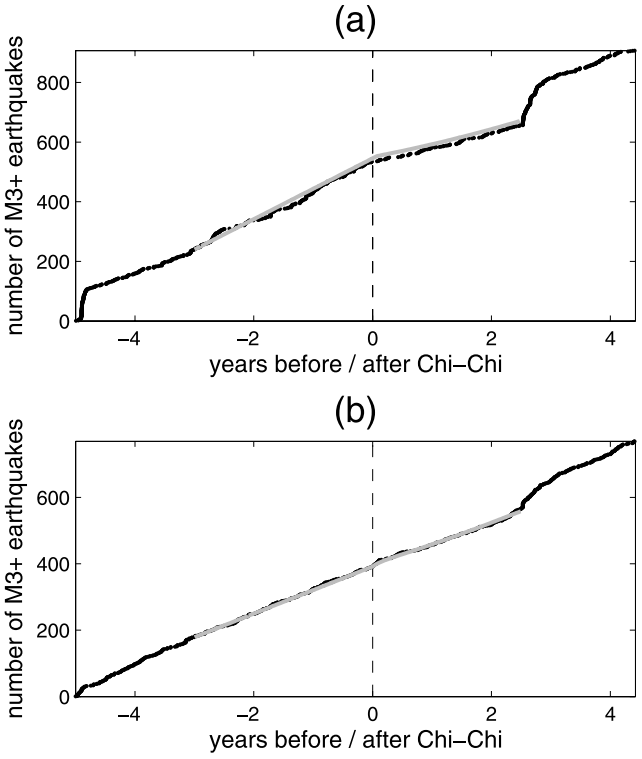

Figure 21. *M*3+ seismicity and best models for the Okinawa Trough, region 6 of Figure 5 for (a) $z < 10$ km and (b) $z > 10$ km. The gray lines are the best models, corresponding to parameters (a) $t_a = 3$ years, $\bar{\tau} = -1$, and $\sigma_\tau = 0.2$; (b) $t_a = 0.4$ year, $\bar{\tau} = -0.3$, and $\sigma_\tau = 1.8$.

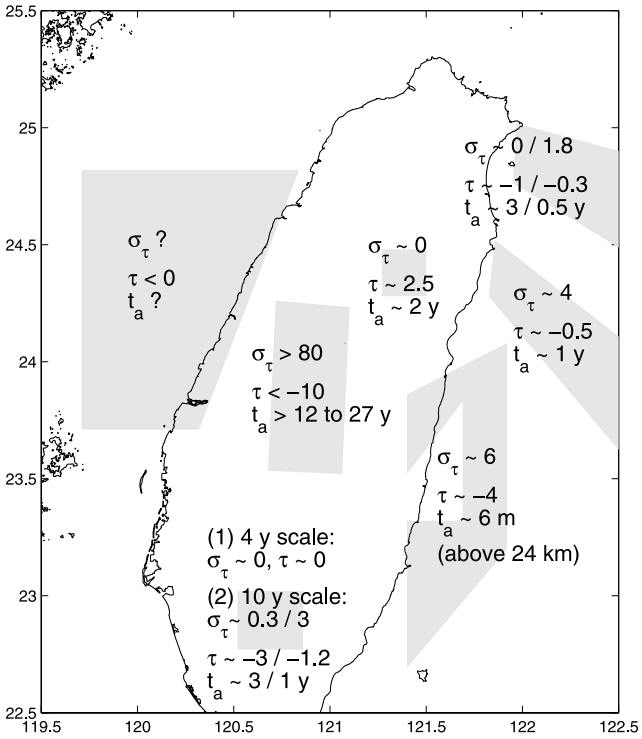

Figure 22. Summary of stress inversion results for Chi-Chi. For Kaoping (south) and Okinawa (north), the two sets of values are for depths less and greater than 10 km.

fault and the influence of the main shock decays. Other triggers than just the main shock itself are then needed both (1) before and (2) after Chi-Chi.

[74] 1. Off-fault prior rates generally appear as not stationary, for example, Figure 10, and this must be properly accounted for when computing rate changes. This was already advocated by *Marsan* [2003] and is certainly the most involved issue in this estimation. Significant changes in earthquake rates prior to Chi-Chi are particularly obvious off-fault, much less so on-fault where the rates appear stable over the 5 years prior to Chi-Chi. Stationarity of the on-fault rate is relative to the very strong rate change caused by Chi-Chi; in order to model on-fault rates, one can neglect small variations occurring before the main shock. When moving away from the Chelungpu fault, the coseismic effect becomes less pronounced, and other comparable triggers must then be accounted for locally.

[75] 2. Local large aftershocks can alter the stress field. It has been shown elsewhere that the total stress imparted by small shocks on pending aftershocks is at least as significant as the stress caused by the main shock (cf. *Marsan* [2005] for such an analysis on the 1992 Landers sequence). The approach followed here does not systematically evaluate the influence of all earthquakes on subsequent activity, as is done with the ETAS model. The nonlinearity of the rate-and-state model complicates this treatment. Instead, we follow a practical method, searching for all the triggers which inclusion improves the Akaike Information Criterion.

[76] The results of our modeling are summarized in Figure 22. Most of the zones, i.e., all except Nansan, experienced a negative mean stress change and therefore eventually exhibit a quiescence, though generally delayed. The on-fault quiescence has yet to be observed. Also, the quiescence in Nansan is clearly not due to Chi-Chi, which on the contrary caused the mean stress to increase in this region. Nansan was found by *Ma et al.* [2005] to experience a positive Coulomb stress change for thrust faults but negative for strike-slip faults. Our result would imply that, if triggering is governed by Coulomb stress, thrust faulting is dominant there. In Taichung and Huathung, the quiescence is well explained by Coulomb modeling, as done by Ma et al. This model however fails at Kaoping, where we find $\bar{\tau} < 0$ (observed at the 10-year scale) while change in Coulomb failure function (ΔCFF) is positive at all depths for both strike-slip and thrust faulting. For Ryukyu and the Okinawa Trough, ΔCFF becomes small, albeit mostly positive in both places.

[77] For Kaoping (10-year scale, $z > 10$ km), Huathung, Ryukyu, and the Okinawa Trough, as well as on the Chelungpu fault itself, the model predicts significant stress variability, i.e., σ_τ greater than or of the order of $|\bar{\tau}|$. In Nansan, the quiescence starts more than 1 year after the main shock and can be well explained by a sudden, heterogeneous stress change which origin is possibly not seismic. For on-fault seismicity, no precise estimate of the stress distribution could be obtained, but lower bounds on σ_τ indicate that the stress heterogeneity is very high there, possibly larger than the mean stress change. This is required by the model to explain triggering lasting more than 4 years on an otherwise coseismic ally unloaded fault. As explained in section 2.3, σ_τ cannot be resolved in case of $\bar{\tau} > 0$, hence for most of the active regions surrounding the Chelungpu fault.

[78] Heterogeneity caused by the spatial variability of slip decays quickly to become negligible at small scales. On the other hand, off-fault coseismic stress heterogeneities can be caused by a variety of mechanisms, in particular related to structural variability. The damage zone surrounding the fault core and complexity in fault geometry are likely to roughen the change in stress imparted by remote earthquakes. Larger scale variability in stress can also be linked to changes in tectonic regime; in the present analysis, large crustal volumes are examined, for which a significant variability in faulting mechanisms can exist. On the basis of the interseismic strain field in Taiwan proposed by *Chang et al.* [2003], the zone with the highest spatial variability in horizontal strain rate tensor (at the $\sim$10-km scale) is seen to extend between the Longitudinal Valley and the Central Range; the strain rate intensity decays quickly, and the mode of deformation switches from shortening to extensional. We therefore examined the seismicity in this zone and how it changed at the time of Chi-Chi. Clear triggering is observed but with no significant stress heterogeneity ($\bar{\tau} = 4.1 \pm 0.4$, $\sigma_\tau = 0 \pm 0.8$, $t_a = 0.4 \pm 0.1$ year) at all depths. The low value of t_a obtained in this inversion should enable us to easily detect a negative change in seismicity rate following Chi-Chi if stress unloading had taken place. The observation that the stress change is spatially uniform over this region is therefore robust. It suggests that the stress heterogeneity that drives earthquake production either acts at scale smaller than the characteristic length of this strain map, or that it is not structurally controlled.

[79] The analysis shows that quite generally, quiescences are more significant and start earlier at shallow depth, in

agreement with a similar obervation by *Ogata et al.* [2003]. This is the case for Taichung, Huathung, the Ryukyu forearc, and Okinawa Trough. Nansan is an exception, since at shallow depth the quiescence started 10 months after being observed at greater depth. Quicker activation of a quiescence could be due to a depth-dependent $A\sigma$ parameter, with lower values of $A\sigma$ implying lower values of t_a. This would be coherent if σ were really the normal stress acting on the fault, hence growing with lithostatic pressure. However, significantly lower values of t_a are on the contrary generally found at greater depth, for example, at Kaoping, Huathung, and the Okinawa Trough. Parameter σ could therefore be better seen as an average with depth of the normal stress.

6. Conclusions

[80] Following the 1999 Chi-Chi earthquake, the seismicity in Taiwan increased substantially as a result of stress transfer from the ruptured Chelungpu fault to nearby faults. While most regions experienced such a triggering of activity, quiescences can also be observed locally although after an initial phase of triggering lasting from days to months/years, depending on the location. This temporal pattern of first triggering then quiescence can be explained by static-stress triggering controlled by rate-and-state friction on the target fault but with distributed static-stress changes. For variable enough stress change distributions, one naturally recovers the observed temporal pattern [*Helmstetter and Shaw*, 2006; *Marsan*, 2006].

[81] Here we asked whether static-stress change distributions can be estimated on- and off-fault, on the basis of the time evolution of the local seismicity. Estimates of the mean and standard deviation can generally be proposed, and the best models are found to reproduce the data very well. A Gaussian model for the static-stress change caused by Chi-Chi is assumed. Significant stress variability is thus measured at various locations, with a particularly strong heterogeneity on the main fault itself where slip heterogeneity is thought to create a very rough stress field.

[82] At the moment, it is still difficult to relate off-fault stress variability to a particular mechanism, especially as the heterogeneity due to large-scale (>10 km) changes in tectonic forcing does not correlate well with the measured stress heterogeneity.

[83] **Acknowledgments.** We would like to thank the associate editor, Elizabeth Cochran, and Sebastian Hainzl for thorough reviews of this paper.

References

Akaike, H. (1973), Information theory as an extension of the maximum likelihood principle, in *2nd International Symposium on Information Theory*, edited by B. N. Petrov and F. Csaksi, 267–281, Akademiai Kiado, Budapest.

Brodsky, E. E. (2006), Long-range triggered earthquakes that continue after the wavetrain passes, *Geophys. Res. Lett.*, *33*, L15313, doi:10.1029/2006GL026605.

Cattin, R., A. Loevenbruck, and X. Le Pichon (2004), Why does the co-seismic slip of the 1999 Chi-Chi (Taiwan) earthquake increase progressively northwestward on the plane of rupture?, *Tectonophysics*, *386*, 67–80.

Chang, C. P, T. Y. Chang, J. Angelier, H. Kao, J. C. Lee, and S. B. Yu (2003), Strain and stress field in Taiwan oblique convergent system: Constraints from GPS observation and tectonic data, *Earth Planet. Sci. Lett.*, *214*, 115–127.

Cochran, E. S., J. E. Vidale, and S. Tanaka (2004), Earth tides can trigger shallow thrust fault earthquakes, *Science*, *306*, 1164–1166.

Daniel, D., D. Marsan, and M. Bouchon (2006), Perturbation of the Izmit earthquake aftershock decaying activity following the 1999 Mw 7.2 Duzce, Turkey, earthquake, *J. Geophys. Res.*, *111*, B05310, doi:10.1029/2005JB003978.

Dieterich, J. H. (1979), Modeling of rock friction: 1. Experimental results and constitutive equations, *J. Geophys. Res.*, *84*, 2161–2168.

Dieterich, J. H. (1986), A model for the nucleation of earthquake slip, in *Earthquake Source Mechanics, Geophys. Monogr. Ser.*, vol. 37, edited by S. Das, J. Boatwright, and C. H. Scholz, pp. 37–47, AGU, Washington, D.C.

Dieterich, J. H. (1994), A constitutive law for rate of earthquake production and its application to earthquake clustering, *J. Geophys. Res.*, *99*, 2601–2618.

Dieterich, J. H., V. Cayol, and P. Okubo (2000), The use of earthquake rate changes as a stress meter at Kilauea volcano, *Nature*, *408*, 457–460.

Dominguez, S., J. P. Avouac, and R. Michel (2003), Horizontal coseismic deformation of the 1999 Chi-Chi earthquake measured from SPOT satellite images: Implications for the seismic cycle along the western foothills of central Taiwan, *J. Geophys. Res.*, *108*(B2), 2083, doi:10.1029/2001JB000951.

Felzer, K. R., and E. E. Brodsky (2005), Testing the stress shadow hypothesis, *J. Geophys. Res.*, *110*(B5), B05S09, doi:10.1029/2004JB003277.

Helmstetter, A., and B. E. Shaw (2006), Relation between stress heterogeneity and aftershock rate in the rate-and-state model, *J. Geophys. Res.*, *111*, B07304, doi:10.1029/2005JB004077.

Helmstetter, A., and D. Sornette (2002), Subcritical and supercritical regimes in epidemic models of earthquake aftershocks, *J. Geophys. Res.*, *107*(B10), 2237, doi:10.1029/2001JB001580.

Huang, W. G., J. H. Wang, B. S. Huang, K. C. Chen, T. M. Chang, R.D. Hwang, H. C. Chiu, and C. C. P. Tsai (2001), Estimates of source parameters for the 1999 Chi-Chi, Taiwan earthquake based on Brune's Source Model, *Bull. Seismol. Soc. Am.*, *91*, 1190–1198.

Hwang, R. D., J. H. Wang, B. S. Huang, K. C. Chen, W. G. Huang, T. M. Chang, H. C. Chiu, and C. C. P. Tsai (2001), Estimates of stress drop of the Chi-Chi, Taiwan earthquake of 20 September 1999 from near-field seismograms, *Bull. Seismol. Soc. Am.*, *91*, 1158–1166.

Iwata, T., H. Sekiguchi, and A. Pitarka (2000), Source and site effects on strong ground motions in near-source area during the 1999 Chi-Chi, Taiwan, earthquake, *Eos Trans. AGU*, *81*, Fall Meet. Suppl., Abstract S72B-07.

Kagan, Y. Y., and H. Houston (2005), Relation between mainshock rupture process and Omori's law for aftershock moment release rate, *Geophys. J. Int.*, *163*, 1039–1048.

Kikuchi, M., Y. Yagi, and Y. Yamanaka (2000), Source process of the Chi-Chi, Taiwan earthquake of Sept. 21, 1999 inferred from teleseismic body waves, Bull. Earthquake Res. Inst., Univ. Tokyo, *75*, pp. 1–13.

Loevenbruck, A., R. Cattin, X. Le Pichon, M. L. Courty, and S. B. Yu (2001), *Seismic Cycle in Taiwan Derived from GPS Measurements*, *333*, 57–64, C.R. Acad. Sci. Paris.

Loevenbruck, A., R. Cattin, X. Le Pichon, S. Dominguez, and R. Michel (2004), Coseismic slip resolution and post-seismic relaxation time of the 1999 Chi-Chi, Taiwan, earthquake as constrained by geological observations, geodetic measurements and seismicity, *Geophys. J. Int.*, *158*, 310–326.

Ma, K. F., T. R. A. Song, S. J. Lee, and H. I. Wu (2000), Spatial slip distribution of the September 20, 1999, Chi-Chi, Taiwan, earthquake (Mw7.6) inverted from teleseismic data, *Geophys. Res. Lett.*, *27*, 3417–3420.

Ma, K. F., J. Mori, S. J. Lee, and S. B. Yu (2001), Spatial and temporal distribution of slip for the 1999 Chi-Chi, Taiwan, earthquake, *Bull. Seismol. Soc. Am.*, *91*, 1069–1087.

Ma, K. F., C. H. Chan, and R. S. Stein (2005), Response of seismicity to Coulomb stress triggers and shadows of the 1999 Mw = 7.6 Chi-Chi, Taiwan, earthquake, *J. Geophys. Res.*, *110*(B5), B05S19, doi:10.1029/2004JB003389.

Mallman, E. P., and M. D. Zoback (2007), Assessing elastic Coulomb stress transfer models using seismicity rates in southern California and southwestern Japan, *J. Geophys. Res.*, *112*, B03304, doi:10.1029/2005JB004076.

Marsan, D. (2003), Triggering of seismicity at short timescales following Californian earthquakes, *J. Geophys. Res.*, *108*(B5), 2266, doi:10.1029/2002JB001946.

Marsan, D. (2005), The role of small earthquakes in redistributing crustal elastic stress, *Geophys. J. Int.*, *163*, 141–151.

Marsan, D. (2006), Can coseismic stress variability suppress seismicity shadows? Insights from a rate-and-state friction model, *J. Geophys. Res.*, *111*, B06305, doi:10.1029/2005JB004060.

Marsan, D., and S. S. Nalbant (2005), Methods for measuring seismicity rate changes: A review and a study of how the M-w 7.3 Landers earthquake affected the aftershock sequence of the M-w 6.1 Joshua Tree earthquake, *Pure Appl. Geophys.*, *162*(6–7), 1151–1185.

Ogata, Y. (2001), Increased probability of large earthquakes near aftershock regions with relative quiescence, *J. Geophys. Res.*, *106*, 8729–8744.

Ogata, Y., and K. Katsura (1993), Analysis of temporal and spatial heterogeneity of magnitude frequency distribution inferred from earthquake catalogues, *Geophys. J. Int.*, *113*, 727–738.

Ogata, Y., L. M. Jones, and S. Toda (2003), When and where the aftershock activity was depressed: Contrasting decay patterns of the proximate large earthquakes in southern California, *J. Geophys. Res.*, *108*(B6), 2318, doi:10.1029/2002JB002009.

Parsons, T. (2002), Global Omori law decay of triggered earthquakes: Large aftershocks outside the classical aftershock zone, *J. Geophys. Res.*, *107*(B9), 2199, doi:10.1029/2001JB000646.

Perfettini, H., and J. P. Avouac (2004), Postseismic relaxation driven by brittle creep: A possible mechanism to reconcile geodetic measurements and the decay rate of aftershocks, application to the Chi-Chi earthquake, Taiwan, *J. Geophys. Res.*, *109*(B2), B02304, doi:10.1029/2003JB002488.

Ruina, A. (1983), Slip instability and state variable friction laws, *J. Geophys. Res.*, *88*, 10,359–10,370.

Shin, T. C., and T. L. Teng (2001), An Overview of the 1999 Chi-Chi, Taiwan earthquake, *Bull. Seismol. Soc. Am.*, *91*, 895–913.

Toda, S., and R. S. Stein (2002), Response of the San Andreas Fault to the 1983 Coalinga-Nuez Earthquakes: An application of interaction-based probabilities for Parkfield, *J. Geophys. Res.*, *107*(B6), 2126, doi:10.1029/2001JB000172.

Toda, S., and S. Stein (2003), Toggling of seismicity by the 1997 Kagoshima earthquake couplet: A demonstration of time-dependent stress transfer, *J. Geophys. Res.*, *108*(B12), 2567, doi:10.1029/2003JB002527.

Toda, S., R. S. Stein, P. A. Reasenberg, J. H. Dieterich, and A. Yoshida (1998), Stress transferred by the 1995 Mw = 6.9 Kobe, Japan, shock: Effect on aftershocks and future earthquake probabilities, *J. Geophys. Res.*, *103*, 24,543–24,565.

Woessner, J., E. Hauksson, S. Wiemer, and S. Neukomm (2004), The 1997 Kagoshima (Japan) earthquake doublet: A quantitative analysis of aftershock rate changes, *Geophys. Res. Lett.*, *31*, L03605, doi:10.1029/2003GL018858.

Yoshioka, S. (2001), Coseismic slip distribution of the 1999 Chi-Chi, Taiwan, Earthquake deduced from inversion analysis of GPS data, *Bull. Seismol. Soc. Am.*, *91*, 1182–1189.

Zhang, W. B., T. Iwata, K. Irikura, H. Sekiguchi, and M. Bouchon (2003), Heterogeneous distribution of the dynamic source parameters of the 1999 Chi-Chi, Taiwan earthquake, *J. Geophys. Res.*, *108*(B5), 2232, doi:10.1029/2002JB001889.

Ziv, A., and A. M. Rubin (2003), Implications of rate-and-state friction for properties of aftershock sequence: Quasi-static inherently discrete simulations, *J. Geophys. Res.*, *108*(B1), 2051, doi:10.1029/2001JB001219.

G. Daniel, Laboratoire de Géophysique Interne et Tectonophysique, Observatoire de Grenoble, 38041 Grenoble Cedex, France. (guillaume.daniel@obs.ujf-grenoble.fr)

D. Marsan, Laboratoire de Géophysique Interne et Tectonophysique, Université de Savoie, 73376 Le Bourget du Lac, France. (david.marsan@univ-savoie.fr)